Further study is needed to extrapolate the species difference *in vivo* from *in vitro* studies. It is important to accumulate the basic research such as the present study when we discuss the extrapolation from animals to human in terms of P-gp function.

ACKNOWLEDGMENTS

We acknowledge Brent Bell for reviewing the manuscript.

REFERENCES

1. Ueda K, Okamura N, Hirai M, Tanigawara Y, Saeki T, Kioka N, Komano T, Hori R. 1992. Human P-glycoprotein transports cortisol, aldosterone, and dexamethasone, but not progesterone. J Biol Chem 267:24248–24252.
2. Schinkel AH, Wagenaar E, van Deemter L, Mol CA, Borst P. 1995. Absence of the mdr1a P-glycoprotein in mice affects tissue distribution and pharmacokinetics of dexamethasone, digoxin, and cyclosporin A. Clin Invest 96:1698–1705.
3. Schinkel AH, Smit JJ, van Tellingen O, Beijnen JH, Wagenaar E, van Deemter L, Mol CA, van der Valk MA, Robanus-Maandag EC, te Riele HP, Berns AJM, Borst P. 1994. Disruption of the mouse mdr1a P-glycoprotein gene leads to a deficiency in the blood-brain barrier and to increased sensitivity to drugs. Cell 77:491–502.
4. Schinkel AH, Mayer U, Wagenaar E, Mol CA, van Deemter L, Smit JJ, van der Valk MA, Voordouw AC, Spits H, van Tellingen O, Zijlmans JM, Fibbe WE, Borst P. 1997. Normal viability and altered pharmacokinetics in mice lacking mdr1-type (drug-transporting) P-glycoproteins. Proc Natl Acad Sci USA 94:4028–4033.
5. Yamazaki M, Neway WE, Ohe T, Chen I, Rowe JF, Hochman JH, Chiba M, Lin JH. 2001. *In vitro* substrate identification studies for P-glycoprotein-mediated transport: Species difference and predictability of *in vivo* results. J Pharmacol Exp Ther 296: 723–735.
6. Tang-Wai DF, Kajiji S, DiCapua F, de Graaf D, Roninson IB, Gros P. 1995. Human (MDR1) and mouse (mdr1, mdr3) P-glycoprotein can be distinguished by their respective drug resistance profiles and sensitivity to modulators. Biochemistry 34: 32–39.
7. Lin JH, Yamazaki M. 2003. Role of P-glycoprotein in pharmacokinetics: Clinical implications. Clin Pharmacokinet 42:59–98.
8. Adachi Y, Suzuki H, Sugiyama Y. 2001. Comparative studies on *in vitro* methods for evaluating *in vivo* function of MDR1 P-glycoprotein. Pharm Res 18:1660–1668.
9. Takeuchi T, Yoshitomi S, Higuchi T, Ikemoto K, Niwa S, Ebihara T, Katoh M, Yokoi T, Asahi S. 2006. Establishment and characterization of the transformants stably-expressing MDR1 derived from various animal species in LLC-PK_1. Pharm Res (in press).
10. Laemmli UK. 1970. Cleavage of structural proteins during the assembly of the head of bacteriophage T4. Nature 227:680–685.
11. Katoh M, Nakajima M, Yamazaki H, Yokoi T. 2000. Inhibitory potencies of 1,4-dihydropyridine calcium antagonists to P-glycoprotein-mediated transport: Comparison with the effects on CYP3A4. Pharm Res 17:1189–1197.
12. Lowry OH, Rosebrough NJ, Farr AL, Randall RJ. 1951. Protein measurement with the Folin phenol reagent. J Biol Chem 193:265–275.
13. Hochman JH, Yamazaki M, Ohe T, Lin JH. 2002. Evaluation of drug interactions with P-glycoprotein in drug discovery: *In vitro* assessment of the potential for drug–drug interactions with P-glycoprotein. Curr Drug Metab 3:257–273.
14. Chen C, Liu X, Smith BJ. 2003. Utility of Mdr1-gene deficient mice in assessing the impact of P-glycoprotein on pharmacokinetics and pharmacodynamics in drug discovery and development. Curr Drug Metab 4:272–291.
15. Polli JW, Wring SA, Humphreys JE, Huang L, Morgan JB, Webster LO, Serabjit-Singh CS. 2001. Rational use of *in vitro* P-glycoprotein assays in drug discovery. J Pharmacol Exp Ther 299:620–628.
16. Saeki T, Ueda K, Tanigawara Y, Hori R, Komano T. 1993. Human P-glycoprotein transports cyclosporin A and FK506. J Biol Chem 268:6077–6080.
17. Georges E, Bradley G, Gariepy J, Ling V. 1990. Detection of P-glycoprotein isoforms by gene-specific monoclonal antibodies. Proc Natl Acad Sci USA 87:152–156.
18. Adachi Y, Suzuki H, Sugiyama Y. 2003. Quantitative evaluation of the function of small intestinal P-glycoprotein: Comparative studies between in situ and *in vitro*. Pharm Res 20:1163–1169.
19. Chiou WL, Jeong HY, Chung SM, Wu TC. 2000. Evaluation of using dog as an animal model to study the fraction of oral dose absorbed of 43 drugs in humans. Pharm Res 17:135–140.
20. He YL, Murby S, Warhurst G, Gifford L, Walker D, Ayrton J, Eastmond R, Rowland M. 1998. Species differences in size discrimination in the paracellular pathway reflected by oral bioavailability of poly(ethylene glycol) and D-peptides. J Pharm Sci 87:626–633.
21. Chiou WL, Buehler PW. 2002. Comparison of oral absorption and bioavailability of drugs between monkey and human. Pharm Res 19:868–874.

22. Yang CP, Cohen D, Greenberger LM, Hsu SI, Horwitz SB. 1990. Differential transport properties of two mdr gene products are distinguished by progesterone. J Biol Chem 265:10282–10288.
23. Yamamoto C, Murakami H, Koyabu N, Takanaga H, Matsuo H, Uchiumi T, Kuwano M, Naito M, Tsuruo T, Ohtani H, Sawada Y. 2002. Contribution of P-glycoprotein to efflux of ramosetron, a 5-HT3 receptor antagonist, across the blood-brain barrier. J Pharm Pharmacol 54:1055–1063.
24. Molden E, Christensen H, Sund RB. 2000. Extensive metabolism of diltiazem and P-glycoprotein-mediated efflux of desacetyl-diltiazem (M1) by rat jejunum *in vitro*. Drug Metab Dispos 28:107–109.
25. Walker DK, Abel S, Comby P, Muirhead GJ, Nedderman AN, Smith DA. 2005. Species differences in the disposition of the CCR5 antagonist, UK-427,857, a new potential treatment for HIV. Drug Metab Dispos 33:587–595.

Available online at www.sciencedirect.com
ScienceDirect
Toxicology Letters 166 (2006) 189–199
Toxicology Letters
www.elsevier.com/locate/toxlet

Dephosphorylation of ribosomal protein P0 in response to troglitazone-induced cytotoxicity

Rawiwan Maniratanachote, Keiichi Minami, Miki Katoh, Miki Nakajima, Tsuyoshi Yokoi *

Drug Metabolism and Toxicology, Division of Pharmaceutical Sciences, Graduate School of Medical Science, Kanazawa University, Kakuma-machi, Kanazawa 920-1192, Japan

Received 25 April 2006; received in revised form 9 July 2006; accepted 10 July 2006
Available online 8 August 2006

Abstract

Troglitazone (TRO)-induced cytotoxicity was investigated in HepG2 cells. The cells were exposed to TRO as well as rosiglitazone (RSG) at concentrations of 0, 25, 50 and 75 μM for 48 h. Total proteins were separated by two-dimensional electrophoresis and visualized by silver staining. We focused on a protein spot at an approximate molecular weight of 35 kDa and isoelectric point (p*I*) of 5.7, which appeared only with the cytotoxic concentrations (50 and 75 μM) of TRO, but not with the low concentration (25 μM) of TRO or any concentrations of RSG. This protein spot was subjected to amino acid sequence analysis and identified as ribosomal protein P0 (P0). Interestingly, without any significant induction of its protein and mRNA, P0 was dephosphorylated depending on the concentration- and time-dependent manner of TRO-induced cytotoxicity. Pretreatment with a general caspase inhibitor, Z-VAD.fmk, prevented cleavage of caspase-3 but demonstrated a slight improvement of cytotoxicity induced by TRO. Thus, these effects could not prevent the dephosphorylation of P0. Our results strongly suggest that a post-translational modification, dephosphorylation, of P0 is associated with TRO-induced cytotoxicity.

Keywords: Troglitazone; Thiazolidinedione; Ribosomal protein P0; Dephosphorylation; Cytotoxicity; Two-dimensional electrophoresis

1. Introduction

Troglitazone (TRO) was the first thiazolidinedione (TZD) approved in 1997 for the treatment of type II diabetes mellitus. This drug showed several therapeutic advantages: it improved hyperinsulinemia and hyperglyceridemia and increased the insulin sensitivity of the target tissues (Fujiwara et al., 1988; Nolan et al., 1994). Several case reports during a few years of utilization strongly supported that TRO could cause severe hepatotoxic effects in some individuals (Gitlin et al., 1998; Neuschwander-Tetri et al., 1998; Shibuya et al., 1998; Watkins and Whitcomb, 1998). Eventually, TRO was withdrawn in 2000.

The antidiabetic effects of TZDs are exerted via the activation of peroxisome proliferator-activated receptorγ (PPARγ) and the potency correlates to their binding activity (Lehmann et al., 1995). However, the toxic effects are unique to TRO since rosiglitazone (RSG), another TZD, shows no clear association with hepatotoxicity (Freid et al., 2000; Isley and Oki, 2000; Lebovitz et al., 2002). Thus, the hepatotoxic effects of TRO are unlikely to be related to a PPARγ class

* Corresponding author. Tel.: +81 76 234 4407; fax: +81 76 234 4407.
E-mail address: TYOKOI@kenroku.kanazawa-u.ac.jp (T. Yokoi).

0378-4274/$ – see front matter © 2006 Elsevier Ireland Ltd. All rights reserved.
doi:10.1016/j.toxlet.2006.07.303

effect. Investigating the mechanisms of TRO-induced hepatotoxicity is difficult because it does not significantly induce liver injury in conventional animal models (Rothwell et al., 2002; Watanabe et al., 1999). However, studies by Funk et al. (2001a,b) demonstrated that TRO and its major metabolite, TRO sulfate, inhibited the ATP-dependent taurocholate transport mediated by the canalicular bile salt export pump (Bsep) in an *in vivo* rat model. The inhibition of Bsep suggests one of possible factors contributing to the hepatotoxicity since subsequent accumulation of bile salts may lead to an intrahepatic cholestasis in humans.

In *in vitro* experiments, TRO has been shown to induce apoptotic cell death in various hepatic cell types (Bae and Song, 2003; Yamamoto et al., 2001). The degree of lethality also depends on the concentration of the agent and the duration of exposure (Bae and Song, 2003; Maniratanachote et al., 2005; Tirmenstein et al., 2002; Yamamoto et al., 2001). In relation to the toxic mechanism, there are several lines of evidences that TRO can cause a decrease in the mitochondrial membrane potential, which is concomitant with a depletion of the cellular ATP concentration (Bova et al., 2005; Tirmenstein et al., 2002), the activation of both c-Jun N-terminal protein kinase (JNK) and p38 kinase, the induction of proapoptotic proteins, Bad and Bax, the release of cytochrome *c* and cleavage of Bid (Bae and Song, 2003) as well as the activation of caspase-3 (Bova et al., 2005; Toyoda et al., 2002).

The purpose of this study is to determine the proteins whose regulation is associated with the toxic effects of TRO in a human hepatoma cell line, HepG2, using a proteomic strategy. We analyzed a protein with an approximate molecular weight (MW) of 35 kDa and isoelectric point (p*I*) of 5.7 that appeared in correlation with the cytotoxic and concentration-dependent exposure to TRO. This protein was identified as ribosomal protein P0 (P0) and found to be dephosphorylated in response to TRO-induced cytotoxicity. The implication of this post-translational modification of P0 by TRO is discussed and its association with the caspase pathway was examined.

2. Materials and methods

2.1. Cell culture condition and treatment of cells

Human hepatoma cell lines, HepG2, obtained from the Riken Gene Bank (Tsukuba, Japan) were maintained in Dulbecco's Modified Eagle's Medium (DMEM, Nissui Pharmaceutical, Tokyo, Japan) containing 10% fetal bovine serum (FBS, BioWhitaker, Walkersville, MD) in a 5% CO_2 atmosphere at 37 °C. TRO and RSG were kindly provided by Sankyo (Tokyo, Japan). Z-VAD.fmk, a general caspase inhibitor, was purchase from Calbiochem (La Jolla, CA). The treated agents were dissolved in DMSO, in which the final concentration did not exceed 0.2%.

2.2. Cell viability assay

HepG2 cells were seeded onto a 96-well plate for 24 h before being treated with 0.1% DMSO, TRO or RSG. Cell viability was assessed by using a Cell Counting Kit-8 assay kit (CCK-8, Dojindo, Kumamoto, Japan) according to the product protocol. The absorbance of the generated formazan product was measured at 450 nm using a microplate reader (Biotrak II, Amersham Biosiences).

2.3. Cell lysate preparation

After treatment, the HepG2 cells were washed twice with PBS and incubated on ice with lysis solution (8 M urea, 4% CHAPS, 2% Pharmalyte 3–10) containing protease inhibitors (1 mM DTT, 0.5 mM APMSF, 2 μg/ml aprotinin, 2 μg/ml pepstatin and 2 μg/ml leupeptin). The cell suspension was placed on ice for 1 h and subsequently centrifuged at 12,000 rpm for 20 min at 4 °C to remove insoluble material. The protein concentration was measured using a Bradford Protein Assay Kit (Bio-Rad Laboratories, Hercules, CA). The cell lysates were stored at −80 °C until the time of analysis.

2.4. Two-dimensional electrophoresis (2-DE)

The devices and chemicals used in 2-DE were purchased from Amersham Biosciences, Buckinghamshire, UK. For the first dimension, 100 μg of protein of the cell lysates were mixed with Destreak Rehydration Solution containing immobilized pH gradient (IPG) buffer of pH 4–7 and applied onto IPG gel strips. The samples were rehydrated at 20 °C for 14 h and subsequently isoelectric focusing (IEF) was performed for a total of 17,500 V h using an Ettan IPGphor Isoelectric Focusing System. IPG strips were subsequently equilibrated with equilibration buffer (50 mM Tris–HCl, pH 8.8, 6 M urea, 30% glycerol and 2% SDS) containing 1% DTT for 15 min and the equilibration buffer containing 2.5% iodoacetamide for 15 min, respectively. The IPG strips were then subjected to the second dimensional electrophoresis using 12% SDS-polyacrylamide slab gels. The two-dimensional gels were stained with 2D-Silver Stain II (Daiichi, Japan) as described in the product protocol.

2.5. Protein identification

The amino acid sequence analyses were performed at Pro Phoenix, Hiroshima, Japan. The protein spot of interest was excised from the silver stained gel of the samples treated with

50 and 75 μM TRO. After in-gel digestion with trypsin, the peptides were reduced and carbamidomethylated. The peptide mass mapping was performed on a MALDI-TOF-TOF and analyzed by LC/MS/MS. The matched peptides were searched using MASCOT (http://www.matrixscience.co.uk) based on the NCBInr database.

2.6. Real-time RT-PCR

At the end of the incubation periods, the cells were washed with PBS and the total RNA was prepared using Isogen® (Nippon Gene, Tokyo, Japan) according to the product protocol. Reverse transcription (RT) reactions were carried out by incubating 2 μg of total RNA with random primer (Takara, Tokyo, Japan) and ReverTraAce (Toyobo, Tokyo, Japan) at 30 °C for 10 min, 42 °C for 60 min and 98 °C for 10 min. Subsequently, the steady state of the mRNA levels was quantified by fluorescence-based real-time RT-PCR. Oligonucleotide sense and antisense primers of human-P0 (5′-AACTCTGCATTCTCGCTTCCTG-3′ and 5′-GACTCTTCCTTGGCTTCAACCT-3′) and GAPDH (5′-CCAGGGCTGCTTTTAACTC-3′ and 5′-GCTCCCCCCTGCAAATGA-3′) were designed to amplify 285 and 292 bp fragments, respectively. The reaction mixture for real-time RT-PCR containing 1 μl of RT product, *Ex Taq* R-PCR Version (Takara, Japan), SYBR® Green I (Molecular Probes, Eugene, OR) and the specific sense and antisense primers were subjected to a Smart Cycler® System (Cepheid, Sunnyvale, CA). After a holding step at 95 °C for 30 s, the thermal cycling was repeated for 45 cycles of 94 °C for 4 s and 64 °C for 20 s followed by melting from 60 to 95 °C at 0.2 °C/s. The standard curve for the relative quantification was created by serially diluted GAPDH concentrations plotted against the threshold cycle number from the real-time PCR reaction. The P0 mRNA expressions were evaluated, and the relative values were normalized with the GAPDH values from the same samples.

2.7. Western blot analysis

The cell lysates were separated by 12% SDS-polyacrylamide gel electrophoresis (PAGE) and transferred to a polyvinylidene fluoride membrane (Immobilon-P, Millipore, Billerica, MA). The specific P0 protein was detected by anti-ribosomal P antibody (HPO-0100, ImmunoVision, Springdale, AR) at a dilution of 1:300. Caspase-3, its precursor and subunits, were detected by anti-caspase-3 antibody (sc-7148, Santa Cruz) at a dilution of 1:200. Biotinylated secondary antibodies and a VECTASTAIN ABC kit (Vector Laboratories, Burlingame, CA) were used. 3,3′-diaminobenzidinetetrahydrochloride (DAB) was used as a substrate for peroxidase. The serine-phosphorylated proteins were detected by anti-phosphoserine antibody (Chemicon, Temecula, CA) at a dilution of 1:600 and a subsequent HRP-conjugated second antibody and were then developed by using an ECL kit (Amersham Biosciences) according to the product protocol.

2.8. In vitro dephosphorylation

Cell lysates at the protein concentration of 100 μg were incubated with 50 units of calf intestinal alkaline phosphatase (CIP, New England Biolabs, Beverly, MA) at 37 °C for 30 min. Subsequently, the cell lysates were subjected to 2-DE and Western blot analysis, respectively.

2.9. Immunoprecipitation

The treated HepG2 cells, about 2×10^7 cells, were lysed in 200 μl of NP-40 lysis buffer (50 mM Tris–HCl, pH 8.0, 150 mM NaCl, 1% Nonidet P-40, 1 mM EDTA, 100 mM NaF, 0.2 mM Na_3VO_4 supplemented with 2 mM APMSF, 50 μg/ml leupeptin and 100 μg/ml aprotinin) for 2 h on ice. The insoluble material was removed by centrifugation at 12,000 rpm for 20 min at 4 °C. To immunoprecipitate the P0, 20 μl of a suspended volume of protein A-agarose (Santa Cruz, Santa Cruz, CA) were incubated with 5 μl of human anti-ribosomal P antibody or normal human serum (negative control) by rotation for 6 h at 4 °C in IP buffer (10 mM Tris–HCl, pH 8.0, 150 mM NaCl, 0.05% Nonidet P-40, 1 mM EDTA, 50 mM NaF and 1 mM Na_3VO_4), followed by cross-linking of the antibody and the beads with dimethylpimelimidate (DMP, Sigma). After washing out the un-cross-linked antibody, the cell lysates (1.2 mg protein) were added to the antibody-bound beads and rotated for 12 h at 4 °C. The beads were washed three times with IP buffer and the immunoprecipitated proteins were eluted with 2% SDS. The proteins were separated by 12% SDS-PAGE before being subjected to Western blot analysis.

2.10. Statistical analysis

Data were analyzed by one-way analysis of variance (ANOVA) followed by Tukey–Kramer multiple comparisons test using Instat Version 2.0 software. Comparison between two groups was made with an unpaired, two-tailed Student's *t*-test. A value of $p < 0.05$ was considered statistically significant.

3. Results

3.1. Troglitazone-induced HepG2 cell toxicity

To investigate cytotoxic effects of TRO, HepG2 cells were exposed to various concentrations of TRO as well as RSG. After 48 h of exposure, TRO caused HepG2 cell toxicity in a concentration-dependent manner (Fig. 1). At 50 and 75 μM TRO markedly reduced the cell viability by 50% and 80% of the control ($p < 0.001$), respectively. RSG showed a significant decrease in cell viability at 25 and 50 μM ($p < 0.05$), but not at 75 μM. At all concentrations of RSG treatment, the cell viability was more than 85% of the control. Therefore, RSG did not have a cytotoxic effect on the HepG2 cells.

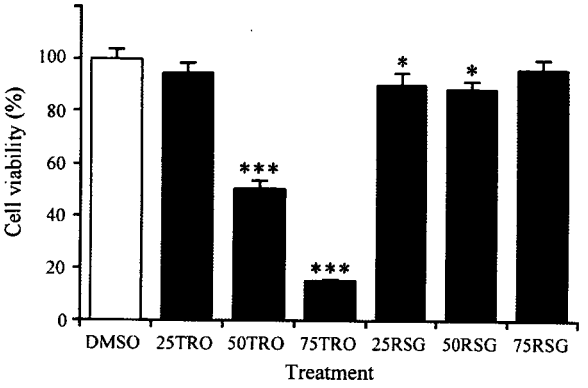

Fig. 1. TRO-induced cytotoxicity. HepG2 were incubated with 0.1% DMSO (control) or the indicated concentration (μM) of TRO or RSG for 48 h. Cell viability was determined by CCK-8 assay. Results represent the mean ± S.D. of three independent experiments. $^{*}p < 0.05$, $^{***}p < 0.001$ compared with the control.

3.2. Proteomic analysis for troglitazone-induced HepG2 cell toxicity

The toxic effects of TRO were further investigated by proteomic analysis. HepG2 cells were treated with 0.1% DMSO (control), various concentrations of TRO or RSG (negative control) for 48 h. The cell lysates were separated by 2-DE and visualized by silver staining. We focused on the spot showing concentration-dependent and TRO-specific changes. The protein of interest was a spot at an approximate MW of 35 kDa and p*I* of 5.7, which appeared only in 50 and 75 μM TRO-treated samples, but not in DMSO, a low concentration (25 μM) of TRO or any concentrations of RSG (Fig. 2A). The spot was excised and subjected to amino acid sequence analysis. The identified amino acid sequences were highly matched with ribosomal protein P0 (P0) (Fig. 2B). This protein had molecular weight and p*I* values near the position that appeared on the two-dimensional gels.

3.3. P0 mRNA and protein expressions by troglitazone treatment

The expressions of P0 mRNA and protein were confirmed by real-time RT-PCR and Western blot analysis using its specific antibody, anti-ribosomal P antibody, respectively. However, neither significant induction of P0 mRNA (Fig. 3A) nor protein expressions (Fig. 3B) was observed.

3.4. Dephosphorylation of P0 by troglitazone-induced toxicity

According to the above results, we then examined whether post-translational modification of P0 caused the different shift in the p*I* by TRO treatment. Therefore, lysates from the cells treated with DMSO or 50 μM TRO for 48 h were separated by 2-DE and detected by Western blot analysis using anti-ribosomal P antibody. Interestingly, it was found that up to five spots of P0 could be identified as indicated by numbers 1–5 which corresponded to approximate p*I* of 5.7, 5.2, 4.8, 4.5 and 4.3, respectively (Fig. 4A, upper-right and -left panels). Treatment of TRO for 48 h caused an increase of the basic components (spots 1 and 2) together with a reduction of more acidic components (spots 3 and 4). Spot 1 was consistent with the spot of interest that appeared on the silver stained two-dimensional gels of the cytotoxic concentrations, 50 and 75 μM, of TRO (Fig. 2A).

It has been well characterized that P0 is a serine-phosphorylated protein (Ballesta et al., 1999; Hasler et al., 1991; Tchórzewski, 2002). In this experiment, P0 underwent *in vitro* dephosphorylation by incubation of the cell lysates with alkaline phosphatase (CIP), which resulted in a p*I* basic-shift showing the similar pattern as that detected with TRO treatment, and the most basic component (spot 0) at a p*I* of about 6.3 was detected (Fig. 4A, lower-right and -left panels). To further confirm the change of phosphorylation, the cell lysates treated with DMSO, 50 μM TRO and 50 μM RSG for 48 h were immunoprecipitated with anti-ribosomal P antibody before being subjected to SDS-PAGE and Western blot analysis. In Fig. 4B, lower panel, lanes 2–4, anti-ribosomal P antibody precipitated a comparable amount of P0 in each sample. As expected, compared to the control, treatment with TRO but not RSG caused a reduction in serine-phosphorylated P0 component (Fig. 4B, upper panel, lanes 2–4). It was also shown that a relatively small amount of P0 was immunoprecipitated by using normal serum from human, a negative control, but its serine phosphorylation could not be clearly detected (Fig. 4B, lane 5). In addition, to determine the phosphorylated spot of P0, the treated cell lysates were subjected to 2-DE and subsequent Western blot analysis using anti-phosphoserine antibody. A number of serine-phosphorylated protein spots, including those other than P0, were detected (data not shown). The corresponding spots of P0 appeared at the same positions as spots 4 and 5, which were more acidic components.

3.5. Time-dependent dephosphorylation of P0 by troglitazone

To evaluate the early dephosphorylation of P0 in correlation to TRO-induced cytotoxicity, HepG2 cells were treated with TRO at the concentration of 75 μM for different times. TRO also caused a time-dependent

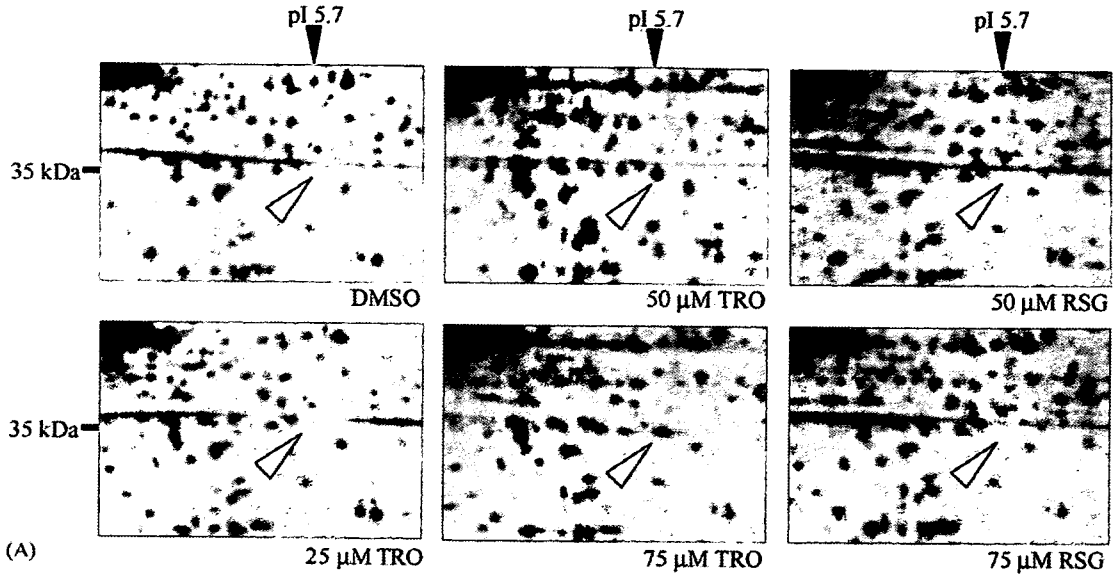

P0

gi|49087144; Total score: 158

Ribosomal protein P0 [Homo sapiens]

Nominal mass (Mr) : 34423

pI : 5.71

```
  1 MPREDRATWK SNYFLKIIQL LDDYPKCFIV GADNVGSKQM QQIRMSLRGK
 51 AVVLMGKNTM MRKAIRGHLE NNPALEKLLP HIRGNVGFVF TKEDLTEIRD
101 MLLANKVPAA ARAGAIAPCE VTVPAQNTGL GPEKTSFFQA LGITTKISRG
151 TIEILSDVQL IKTGDKVGAS EATLLNMLNI SPFSFGLVIQ QVFDNGSIYN
201 PEVLDITEET LHSRFLEGVR NVASVCLQIG YPTVASVPHS IINGYKRVLA
251 LSVETDYTFP LAEKVKAFLA DPSAFVAAAP VAAATTAAPA AAAAPAKVEA
(B) 301 KEESEESDED MGFGLFD
```

Fig. 2. Protein expression profiles of two-dimensional gels from silver staining and amino acid sequence analyses. (A) HepG2 cells were incubated with 0.1% DMSO (control) or various concentrations of TRO or RSG for 48 h. The cell lysates were separated by 2-DE and visualized by silver staining. The protein of interest which appeared in relation to TRO-induced cytotoxicity was located at an approximate MW of 35 kDa and p*I* of 5.7 (arrow head). (B) The protein spot of interest was excised from the silver stained gel of the samples treated with 50 and 75 μM TRO and subjected to amino acid sequence analyses. The 'bold underlined' sequences denote peptides, which matched with ribosomal protein P0.

cytotoxicity (Fig. 5A). After 4 h of exposure, comparing to the control (DMSO), cell viability was significantly reduced ($p < 0.05$). Cell lysates were separated by 2-DE and detected by Western blot analysis using anti-ribosomal P antibody. According to the profiles, the p*I* basic-shift of P0 demonstrated in a time-dependent manner that spot 1, which is a dephosphorylated component, appeared after 4 h of TRO treatment (Fig. 5B).

3.6. Effect of caspase inhibition on troglitazone-induced cytotoxicity and P0 dephosphorylation

To further investigate the involvement of caspase activation and dephosphorylation of P0, a general caspase inhibitor (Z-VAD.fmk) was used to pretreat HepG2 cells for 2 h before they were exposed to TRO. In our study, pretreatment with Z-VAD.fmk at concentrations of 50–200 μM significantly improved the HepG2 cell viability from approximately 60% to 80%, and the viability improved from 25% to 60% with 75 and 100 μM of TRO treatment ($p < 0.01$), respectively, for as long as 6 h (Fig. 6A). Western blot results demonstrated that treatment of the HepG2 cells with 75 and 100 μM TRO caused an activation of caspase-3 as shown by two cleavage subunits of caspase-3 at MW of 20 and 17 kDa, respectively. These subunits were absent in the cells pretreated with Z-VAD.fmk (Fig. 6B). However, the protective effect of the caspase inhibitor could not prevent the p*I* shift of P0 in

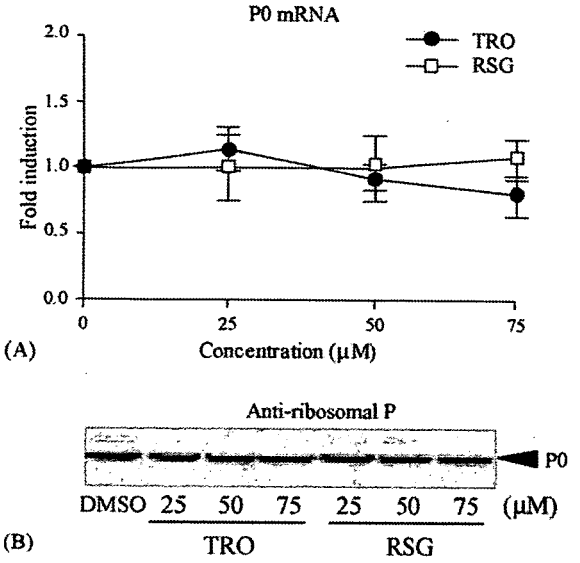

Fig. 3. P0 mRNA and protein expressions. (A) HepG2 cells treated with 0.1% DMSO (control) or various concentrations of TRO or RSG for 48 h were subjected to real-time RT-PCR. Results represent the mean ± S.D. of three independent experiments. (B) The cell lysates were subjected to Western blot analysis using anti-ribosomal P antibody. Two additional Western blot analyses yielded equivalent results.

75 μM TRO-treated HepG2 cells for neither 4 h nor 6 h (Fig. 6C).

3.7. Effect of hydrogen peroxide on cell viability and P0 dephosphorylation

Above results showed that inhibition of the caspases could not prevent the dephosphorylation of P0. We additionally investigated the effect of necrotic cell death on the dephosphorylation of P0 using H_2O_2 as a treating agent. Since the toxic effects induced by H_2O_2 is highly concentration- and cell type-dependent response, in this study, HepG2 cells were treated with the increasing concentrations of H_2O_2 for 24 h before measurement of cell viability by CCK-8. As demonstrated in Fig. 7A, the cell viability was dramatically reduced with the concentrations of H_2O_2 higher than 0.5 mM ($p < 0.001$). The cell lysates of these treated HepG2 cells were subjected to immunoprecipitation with anti-ribosomal P and Western blot analysis. A reduction of serine-phosphorylated P0 was detected with 0.5 mM H_2O_2 treatment but not with a higher concentration of 1 mM (Fig. 7B). However, with higher concentrations of H_2O_2 (2 and 4 mM), which having about 10% cell viability, the serine-phosphorylated P0 extent was gradually reduced.

4. Discussion

Troglitazone was the first TZD agent for treating type II diabetes mellitus. This drug was withdrawn from the market because of severe hepatotoxicity (Gitlin et al., 1998; Neuschwander-Tetri et al., 1998; Shibuya et al., 1998; Watkins and Whitcomb, 1998). In this study, cytotoxicity of TRO was investigated in a human hepatoma cell line, HepG2. As shown in Fig. 1, treatment of the cells for 48 h with TRO demonstrated a concentration-dependent cytotoxicity whereas only a slight cytotoxicity was found with RSG treatment. These results were consistent with our previous reports (Maniratanachote et al., 2005; Yamamoto et al., 2001) and the lethal effects of TRO are exemplified by apoptosis (Bae and Song, 2003; Toyoda et al., 2002; Yamamoto et al., 2001). Using a proteomic strategy for determining the critical protein expression in the profiles, the protein of interest was a spot at an approximate MW of 35 kDa and p*I* of 5.7 (Fig. 2A). This spot appeared in the profiles after treatment only with the cytotoxic concentrations (50 and 75 μM) of TRO, but not with the low concentration (25 μM) of TRO or any concentrations of RSG. The spot was identified as ribosomal protein P0 (P0) (Fig. 2B).

P0 is a component of eukaryotic ribosomal stalk, which anchors two copies of P1 and P2 to form a pentameric complex and is associated with the 60S ribosomal subunit (Gonzalo et al., 2001; Gonzalo and Reboud, 2003; Remacha et al., 1995; Rich and Stietz, 1987; Tchórzewski, 2002). The ribosomal P protein complex interacts with 28S rRNA forming a GTPase domain, which is active during the elongation step of protein translation (Gonzalo and Reboud, 2003). In previous reports, P0 mRNA was overexpressed in hepatocellular carcinoma and colon carcinoma in human (Barnard et al., 1992) as well as in cultured rat thyroid cells after phorbol ester treatment suggesting an association with cell growth and proliferation (Saito et al., 1994). In our study, although the 2-DE profiles of P0 in relation to TRO-induced cytotoxicity were clearly different from those of the control, the mRNA and protein were not significantly induced as shown in Fig. 3A and B, respectively. Two acidic ribosomal protein partners of P0, P1 and P2, exhibit a high acidic property with a p*I* of 3–4 (Ballesta et al., 1999; Tchórzewski, 2002). Accordingly, they could not be detected in the p*I* range of 4–7 used in this study. Nevertheless, in the SDS-PAGE/Western blot analysis, an upper band at an approximate MW of 35 kDa and two lower bands at MW between 20 and 15 kDa were detected (Fig. 3B and data not shown) which correspond to P0, P1 and P2, respectively (Gonzalo et al., 2001). P1 and P2 components were also equally expressed in

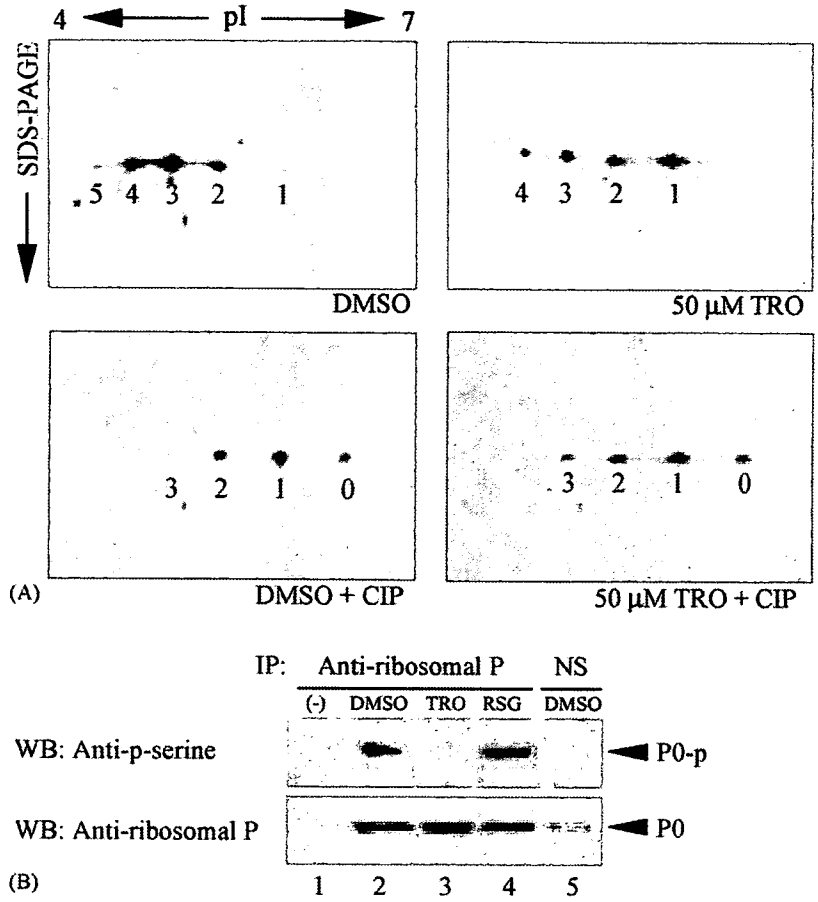

Fig. 4. Dephosphorylated shift of P0 spots detected by 2-DE and Western blot analysis. (A) HepG2 cell lysates treated with 0.1% DMSO (upper-left panel) or 50 μM TRO (upper-right panel) were separated by 2-DE and subsequent Western blot analysis using anti-ribosomal P antibody. The same treated cell lysates were incubated with 50 IU of CIP for 37 °C for 30 min before being subjected to 2-DE and Western blot analysis using anti-ribosomal P antibody (lower-left and -right panels). The spot numbers of 0–5 corresponded to approximate p*I* of 6.3, 5.7, 5.2, 4.8, 4.5 and 4.3, respectively. (B) HepG2 cells were treated with DMSO, 50 μM TRO and 50 μM RSG for 48 h (lanes 2–5). P0 was immunoprecipitated with anti-ribosomal P antibody (lanes 1–4). Normal serum from human was used as an immunoprecipitated-negative control (lane 5). About 20 and 5 μl of precipitates were detected with anti-phosphoserine antibody (upper panel) or anti-ribosomal P antibody (lower panel), respectively. Lane 1(−) is a negative control to which no cell lysate was applied. WB, Western blot; IP, immunoprecipitation; NS, normal serum; Anti-p-serine, anti-phosphoserine; P0-p, phosphorylated P0.

all treatments (data not shown). These results allowed us to focus on a post-translational modification of P0 in response to TRO-induced cytotoxicity.

It is known that mammalian ribosomal P proteins can be phosphorylated both *in vitro* and *in vivo* at the conserved C-terminal region on the serine residues (Ballesta et al., 1999; Hasler et al., 1991; Tchórzewski, 2002) by several kinases such as casein kinase 2 (CK2), a family of RAP kinases and a specific kinase PK60 (Ballesta et al., 1999; Hasler et al., 1991). In an agreement with its characterization as a phosphoprotein, the p*I* heterogeneity was observed for P0 and was further shifted to a more basic p*I* after *in vitro* incubation of the cell lysates with protein phosphatase, CIP (Fig. 4A). In addition, we confirmed that P0 was dephosphorylated after TRO treatment as shown in Fig. 4B and further found that the more acidic spots, 4 and 5, were the serine-phosphorylated P0 components (data not shown). Thus, spot 1 that appeared with 50 and 75 μM of TRO treatment in HepG2 cells corresponded to a dephosphorylated form of P0. Moreover, the time-dependent relation of cytotoxicity of TRO and dephosphorylation of P0 could be observed after 4 h of 75 μM of TRO exposure (Fig. 5). These results confirmed that P0 was dephosphorylated in response to TRO-induced cytotoxicity.

In relation to the cytotoxicity, dephosphorylation of ribosomal P proteins also occurs during Fas-L induced apoptosis in Jurkat cells (Zampieri et al., 2001). Moreover, a shift of the P0 spot toward basic p*I* is associated with apoptosis induced by anti-IgM antibody

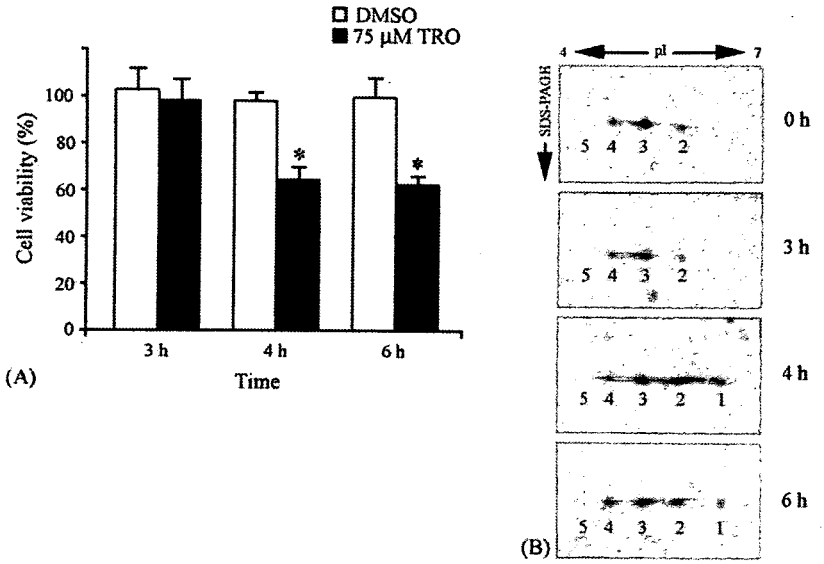

Fig. 5. Time-dependent cytotoxicity of TRO and P0 dephosphorylation. (A) HepG2 cells were treated with 0.1% DMSO (control) or 75 μM TRO for the time indicated. Cell viability was determined by CCK-8 assay. Results represent the mean ± S.D. of three independent experiments. $^{*}p < 0.05$ compared with the control of the corresponded time. (B) HepG2 cells treated with 75 μM TRO for 0–6 h were subjected to 2-DE and subsequent to Western blot analysis using anti-ribosomal P antibody. The spot numbers 1–5 corresponded to the approximate p*I* of 5.7, 5.2, 4.8, 4.5 and 4.3, respectively.

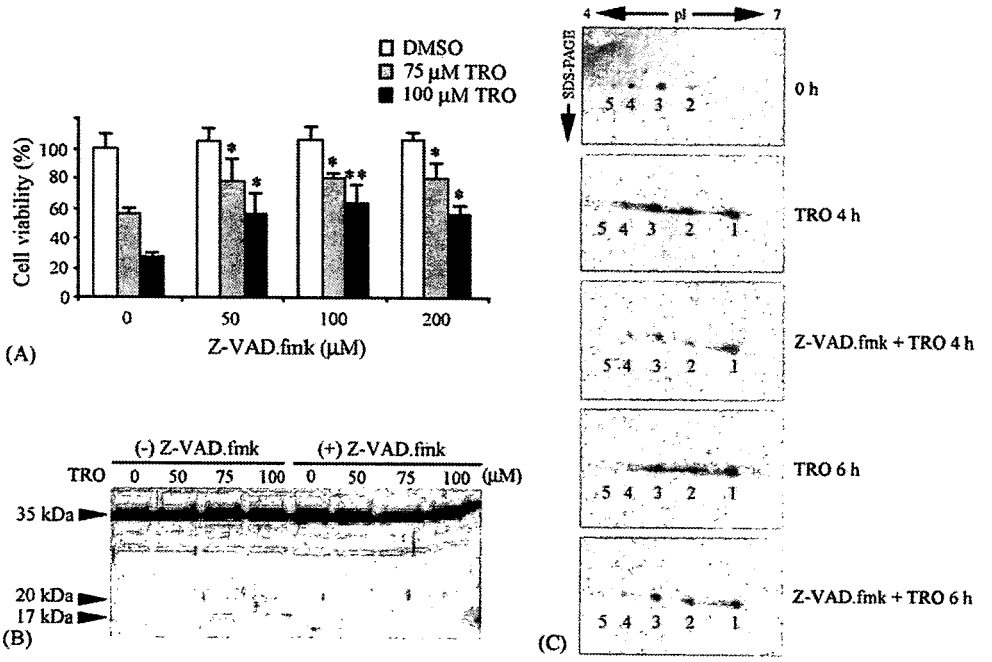

Fig. 6. Prevention of TRO-induced toxicity and cleavage of caspase-3 by general caspase inhibitor. (A) HepG2 cells were pretreated with various concentrations of Z-VAD.fmk, a general caspase inhibitor, for 2 h before being treated with the indicated concentration of TRO or 0.1% DMSO for 6 h. Cell viability was determined by CCK-8. Results represent the mean ± S.D. of three independent experiments. $^{*}p < 0.05$, $^{**}p < 0.01$ compared with the pretreated control (0 μM Z-VAD.fmk) of the corresponded treatment. (B) HepG2 cells were pretreated without or with Z-VAD.fmk for 2 h before being treated with TRO or DMSO for 4 h. The cell lysates were subjected to Western blot analysis using anti-caspase-3 antibody. (C) HepG2 cells were pretreated without or with Z-VAD.fmk for 2 h before being treated with 75 μM TRO for 4 h or 6 h. The cell lysates were subjected to 2-DE and subsequent Western blot analysis using anti-ribosomal P antibody. The spot numbers 1–5 corresponded to the approximate p*I* of 5.7, 5.2, 4.8, 4.5 and 4.3, respectively.

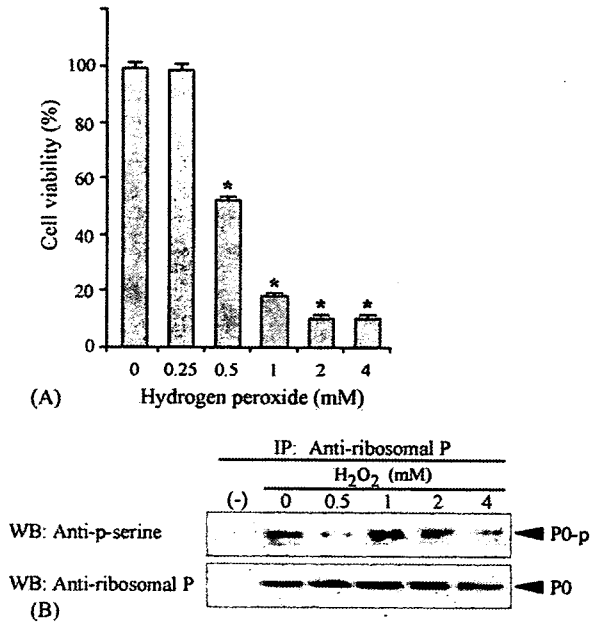

Fig. 7. Effects of hydrogen peroxide on HepG2 cell viability and P0 dephosphorylation. (A) HepG2 cells were treated with various concentrations of H_2O_2 for 24 h. Cell viability was determined by CCK-8. Results represent the mean ± S.D. of three independent experiments. $^*p < 0.001$ compared with 0 mM H_2O_2. (B) P0 was immunoprecipitated with anti-ribosomal P antibody. About 20 and 5 μl of precipitates were detected with anti-phosphoserine antibody (upper panel) or anti-ribosomal P antibody (lower panel), respectively. Lane 1(−) is a negative control to which no cell lysate was applied. WB, Western blot; IP, immunoprecipitation; Anti-p-serine, anti-phosphoserine; P0-p, phosphorylated P0.

in human Burkitt lymphoma cell lines (Brockstedt et al., 1998). In those studies, P0 was identified as an apoptosis-associated protein since the modification of this protein is correlated with the activity of the caspase pathway, which can be prevented by caspase inhibitors (Brockstedt et al., 1998; Zampieri et al., 2001). The caspase pathway, especially for an activation of caspase-3, is known to be involved in TRO-induced apoptosis (Bova et al., 2005; Toyoda et al., 2002). We, therefore, investigated the association between dephosphorylation of P0 and TRO-induced cytotoxicity in relation to this mechanism. It was found that Z-VAD.fmk pretreatment significantly improved the cell viability in TRO-treated HepG2 cells (Fig. 6A). However, the protective effects of this caspase inhibitor could not completely quench out the cytotoxic effects of TRO, even with the increased concentrations (50–200 μM) of Z-VAD.fmk. In addition, the results from Western blot analysis demonstrated that treatment of TRO caused a slight cleavage of caspase-3, which could be totally eliminated by Z-VAD.fmk pretreatment (Fig. 6B). These results indicated that the activation of caspase was partly involved in TRO cytotoxicity and gave a reasonable explanation why pretreatment of HepG2 cells with Z-VAD.fmk could not prevent the dephosphorylation of P0 (Fig. 6C). Bae and Song (2003) reported strong evidence that c-Jun N-terminal kinase (JNK)-mediated cell death pathway plays a critical role in TRO-induced cytotoxicity. However, inhibition of JNK activation by pretreatment the cells with SP600125 did not overcome the dephosphorylation of P0 in our observation (data not shown). The dephosphorylation of P0 by TRO may be associated in concert with several cell death-mediated pathways, which await thorough investigations.

In previous reports, the most likely cell death mechanism induced by TRO is via apoptosis (Bae and Song, 2003; Toyoda et al., 2002; Yamamoto et al., 2001). However, TRO has shown to disrupt mitochondrial functions and to induce a depletion of ATP in the cells (Bova et al., 2005; Tirmenstein et al., 2002). Under these toxic conditions, necrosis component of cell death might take place (Lemasters et al., 1998). To investigate whether necrotic cell death is associated with the dephosphorylation of P0, H_2O_2, an oxidative stress inducer, was used as a model reagent. Mode of cell death induced by this reagent suggests a highly concentration- and cell type-dependent response. At low concentrations, H_2O_2 induced the mode of apoptosis, while at higher levels of oxidative stress, the mode is switched to necrosis (Csordas et al., 2006; Lee and Shacter, 1999; Palomba et al., 1999). In Fig. 7A, we showed that with 0.05 mM H_2O_2 caused about 50% cell viability. This suggests the both modes of cell death, apoptosis and necrosis (Csordas et al., 2006; Lee and Shacter, 1999). In addition, cleavage of caspase-3 was also observed (data not shown). Consistently with the toxicity induced by TRO (Fig. 4B), the serine-phosphorylated P0 extent was decreased with 0.5 mM H_2O_2 (Fig. 7B). In contrast, the extent of P0 phosphorylation with 1 mM H_2O_2 was comparable to the control. Such a cell viability as low as about 20% caused by 1 mM H_2O_2, the prominent mode of cell death has been suggested to be a necrosis (Csordas et al., 2006; Lee and Shacter, 1999). Therefore, dephosphorylation of P0 by TRO and 0.5 mM H_2O_2 was likely associated with a sufficient level of apoptosis rather than necrosis.

During apoptosis, one of the cellular responses is the regulation of protein translation, which is divided into three distinct phases: initiation, elongation and termination (Holcik and Sonenberg, 2005). In previous reports, TRO has been shown to promote calcium release from the endoplasmic reticulum leading to phosphorylation of eukaryotic initiation factor 2α (eIF2α) followed by the inhibition of translation initiation (Gardner et al., 2005; Palakurthi et al., 2001). In yeast, phosphorylation

of P0 has been suggested to affect the translation of specific mRNAs that can have some important phenotypic consequences in some specific conditions (Rodriguez-Gabriel et al., 1998). Unfortunately, at present, no definite mechanism has been established for the phosphorylation or dephosphorylation of P0 in relation to toxicity. Our results, however, strongly suggest that P0 is associated with TRO-induced cytotoxicity. Dephosphorylation of P0, which could not be prevented by the caspase inhibition, may play a role in the regulation of protein translation in response to the toxic effects of TRO.

Acknowledgments

This work was supported in part by Research on Advanced Medical Technology, Health and Labor Science Research Grants from the Ministry of Health, Labor and Welfare of Japan. We thank Mr. Brent Bell for reviewing the manuscript.

References

Bae, M.A., Song, B.J., 2003. Critical role of c-Jun N-terminal protein kinase activation in troglitazone-induced apoptosis of human HepG2 hepatoma cells. Mol. Pharmacol. 63, 401–408.

Ballesta, J.P.G., Rodriguez-Gabriel, M.A., Bou, G., Briones, E., Zambrano, R., Remacha, M., 1999. Phosphorylation of the yeast ribosomal stalk. Functional effects and enzymes involved in the process. FEMS Microbiol. Rev. 23, 537–550.

Barnard, G.F., Staniunas, R.J., Bao, S., Mafune, K., Steele Jr., G.D., Gollan, J.L., Chen, B.L., 1992. Increase expression of human ribosomal phosphoprotein P0 messenger RNA in hepatocellular carcinoma and colon carcinoma. Cancer Res. 52, 3067–3072.

Bova, M.P., Tam, D., McMahon, G., Mattson, M.N., 2005. Troglitazone-induces a rapid drop of mitochondrial membrane potential in liver HepG2 cells. Toxicol. Lett. 155, 41–50.

Brockstedt, E., Rickers, A., Kostka, S., Laubersheimer, A., Döken, B., Wittmann-Liebold, B., Bommert, K., Otto, A., 1998. Identification of apoptosis-associated proteins in a human Burkitt lymphoma cell line. J. Biol. Chem. 273, 28057–28064.

Csordas, A., Wick, G., Bernhard, D., 2006. Hydrogen peroxide-mediated necrosis induction in HUVECs is associated with an atypical pattern of caspase-3 cleavage. Exp. Cell Res. 312, 1753–1764.

Freid, J., Everitt, D., Boscia, J., 2000. Rosiglitazone and hepatic failure. Ann. Intern. Med. 132, 164.

Fujiwara, T., Yoshioka, S., Yoshioka, T., Ushiyama, I., Horikoshi, H., 1988. Characterization of new oral antidiabetic agent CS-045: studies in KK and ob/ob mice and Zucker fatty rats. Diabetes 37, 1549–1558.

Funk, C., Pantze, M., Jehle, L., Ponelle, C., Scheuermann, G., Lazendic, M., Gasser, R., 2001a. Troglitazone-induced intrahepatic cholestasis by an interference with the hepatobiliary export of the bile acids in male and female rats. Correlation with the gender difference in troglitazone sulfate formation and the inhibition of the canalicular bile salt export pump (Bsep) by troglitazone and troglitazone sulfate. Toxicology 167, 83–98.

Funk, C., Ponelle, C., Scheuermann, G., Pantze, M., 2001b. Cholestatic potential of troglitazone as a possible factor contributing to troglitazone-induced hepatotoxicity: in vivo and in vitro interaction at the canalicular bile salt export pump (Bsep) in the rat. Mol. Pharmacol. 59, 627–635.

Gardner, O.S., Shiau, C.W., Chen, C.S., Graves, L.M., 2005. Peroxisome proliferator-activated receptory-independent activation of p38 MAPK by troglitazone involves calcium/calmodulolin-dependent protein kinase II and protein kinase R: correlation with endoplasmic reticulum stress. J. Biol. Chem. 280, 10109–10118.

Gitlin, N., Julie, N.L., Spurr, C.L., Lim, K.N., Juarbe, H.M., 1998. Two cases of severe clinical and histologic hepatotoxicity associated with troglitazone. Ann. Intern. Med. 129, 36–38.

Gonzalo, P., Lavergne, J.P., Reboud, J.P., 2001. Pivotal role of the P1 N-terminal domain in the assembly of the mammalian ribosomal stalk and in the proteosynthetic activity. J. Biol. Chem. 276, 19762–19769.

Gonzalo, P., Reboud, J.P., 2003. The puzzling lateral flexible stalk of the ribosome. Biol. Cell 95, 179–193.

Hasler, P., Brot, N., Weissbach, H., Parnassa, A.P., Elkon, K.B., 1991. Ribosomal proteins P0, P1 and P2 are phosphorylated by casein kinase II at their conserved carboxyl termini. J. Biol. Chem. 266, 13815–13820.

Holcik, M., Sonenberg, N., 2005. Translational control in stress and apoptosis. Nat. Rev. Mol. Cell Biol. 6, 318–327.

Isley, W.L., Oki, J.C., 2000. Rosiglitazone and liver failure. Ann. Intern. Med. 133, 393.

Lebovitz, H.E., Kreider, M., Freed, M.I., 2002. Evaluation of liver function in type 2 diabetic patients during clinical trials. Diabetes Care 25, 815–821.

Lee, Y.J., Shacter, E., 1999. Oxidative stress inhibits apoptosis in human lymphoma cells. J. Biol. Chem. 274, 19792–19798.

Lehmann, J.M., Moore, L.B., Smith-Oliver, T.A., Wilkison, W.O., Willson, T., Kliewer, S.A., 1995. An antidiabetic thiazolidinedione is a high affinity ligand for peroxisome-activated receptor γ (PPARγ). J. Biol. Chem. 270, 12953–12956.

Lemasters, J.J., Nieminen, A.L., Qian, T., Trost, L.C., Elmore, S.P., Nishimura, Y., Crowe, R.A., Cascio, W.E., Bradham, C.A., Brenner, D.A., Herman, B., 1998. The mitochondrial permeability transition in cell death: a common mechanism in necrosis, apoptosis and autophagy. Biochim. Biophys. Acta 1366, 177–196.

Maniratanachote, R., Minami, K., Katoh, M., Nakajima, M., Yokoi, T., 2005. Chaperone proteins involved in troglitazone-induced toxicity in human hepatoma cell lines. Toxicol. Sci. 83, 293–302.

Neuschwander-Tetri, B.A., Isley, W.L., Oki, J.C., Ramrakhiani, S., Quiason, S.G., Phillips, N.J., Brunt, E.M., 1998. Troglitazone-induced hepatic failure leading to liver transplantation. Ann. Intern. Med. 129, 38–41.

Nolan, J.J., Ludvik, B., Beerdsen, P., Joyce, M., Olefsky, J., 1994. Improvement in glucose tolerance and insulin resistance in obese subjects treated with troglitazone. N. Engl. J. Med. 331, 1188–1193.

Palakurthi, S.S., Aktas, H., Grubissich, L.M., Mortensen, R.M., Halperin, J.A., 2001. Anticancer effects of thaiazolidinediones are independent of peroxisome proliferators-activated receptor γ and mediated by inhibition of translation initiation. Cancer Res. 61, 6213–6218.

Palomba, L., Sestili, P., Columbaro, M., Falcieri, E., Cantoni, O., 1999. Apoptosis and necrosis following exposure of U937 cells to increasing concentrations of hydrogen peroxide: the effect of the poly (ADP-ribose) polymerase inhibitor 3-aminobenzamide. Biochem. Pharmacol. 58, 1743–1750.

Remacha, M., Jimenez-Diaz, A., Santos, C., Briones, E., Zambrano, R., Gabriel, M.A.R., Guarinos, E., Ballesta, J.P.G., 1995. Proteins

P1, P2, and P0, components of the eukaryotic ribosome stalk. New structural and functional aspects. Biochem. Cell Biol. 73, 959–968.

Rich, B.E., Stietz, J.A., 1987. Human acidic ribosomal phosphoproteins P0, P1 and P2: analysis of cDNA clones, in vitro synthesis, and assembly. Mol. Cell Biol. 7, 4065–4074.

Rodriguez-Gabriel, M.A., Remacha, M., Ballesta, J.P.G., 1998. Phosphorylation of ribosomal protein P0 is not essential for ribosome function but can affect translation. Biochemistry 37, 16620–16626.

Rothwell, C., McGuire, E.J., Altrogge, D.M., Masuda, H., de la Iglesia, F.A., 2002. Chronic toxicity in monkeys with the thiazolidinedione antidiabetic agent troglitazone. J. Toxicol. Sci. 27, 35–47.

Saito, T., Ikeda, M., Endo, T., Tsurugi, K., Onaya, T., 1994. Increased expression of acidic ribosomal protein (P0) mRNA after phorbol ester treatment of cultured rat thyroid (FRTL-5) cells. Biochem. Biophys. Res. Commun. 203, 780–788.

Shibuya, A., Watanabe, M., Fujita, Y., Saigenji, K., Kuwao, S., Takahashi, H., Takeuchi, H., 1998. An autopsy case of troglitazone-induced fulminant hepatitis. Diabetes Care 21, 2140–2143.

Tchórzewski, M., 2002. The acidic ribosomal P proteins. Int. J. Biochem. Cell Biol. 34, 911–915.

Tirmenstein, M.A., Hu, C.X., Gales, T.L., Maleeff, B.E., Narayanan, P.K., Kurali, E., Hart, T.K., Thomas, H.C., Schwartz, L.W., 2002. Effects of troglitazone on HepG2 viability and mitochondrial function. Toxicol. Sci. 69, 131–138.

Toyoda, M., Takagi, H., Horiguchi, N., Kakizaki, S., Sato, K., Takayama, K., Mori, M., 2002. A ligand for peroxisome proliferator activated receptor γ inhibits cell growth and induces apoptosis in human liver cancer cells. Gut 50, 563–567.

Watanabe, T., Ohashi, Y., Yasuda, M., Takaoka, M., Furukawa, T., Yamoto, T., Sanbuissho, A., Manabe, S., 1999. Was it possible to predict liver dysfunction caused by troglitazone during the non-clinical safety studies? Iyakuhin Kenkyu 30, 537–546.

Watkins, P.B., Whitcomb, R.W., 1998. Hepatic dysfunction associated with troglitazone. N. Engl. J. Med. 338, 916–917.

Yamamoto, Y., Nakajima, M., Yamazaki, H., Yokoi, T., 2001. Cytotoxicity and apoptosis produced by troglitazone in human hepatoma cells. Life Sci. 70, 471–482.

Zampieri, S., Degen, W., Ghirardello, A., Doria, A., van Venrooij, W.J., 2001. Dephosphorylation of autoantigenic ribosomal P proteins during Fas-L induced apoptosis: a possible trigger for the development of the autoimmune response in patients with systemic lupus erythematosus. Ann. Rheum. Dis. 60, 72–76.

MicroRNA Regulates the Expression of Human Cytochrome P450 1B1

Yuki Tsuchiya,[1] Miki Nakajima,[1] Shingo Takagi,[1] Takao Taniya,[2] and Tsuyoshi Yokoi[1]

[1]Drug Metabolism and Toxicology, Division of Pharmaceutical Sciences, Graduate School of Medical Science, Kanazawa University; and [2]Futaba Breast Clinic, Kanazawa, Japan

Abstract

MicroRNAs (miRNA) are small noncoding RNAs that regulate gene expression through translational repression or mRNA cleavage. Here, we found that cytochrome P450 (CYP), a superfamily of drug-metabolizing enzymes, is a target of miRNA. Human CYP1B1, which is highly expressed in estrogen target tissues, catalyzes the metabolic activation of various procarcinogens and the 4-hydroxylation of 17β-estradiol. CYP1B1 protein is abundant in cancerous tissues. We identified a near-perfect matching sequence with miR-27b in the 3′-untranslated region of human CYP1B1. Luciferase assays revealed that the reporter activity of the plasmid containing the miR-27b recognition element was decreased in MCF-7 cells (miR-27 positive) but not in Jurkat cells (miR-27b negative). Exogenously expressed miR-27b could decrease the luciferase activity in Jurkat cells. In MCF-7 cells, the antisense oligoribonucleotide for miR-27b restored the luciferase activity and increased the protein level and enzymatic activity of endogenous CYP1B1. These results suggested that human CYP1B1 is post-transcriptionally regulated by miR-27b. The expression levels of miR-27b and CYP1B1 protein in breast cancerous and adjacent noncancerous tissues from 24 patients were evaluated. In most patients, the expression level of miR-27b was decreased in cancerous tissues, accompanied by a high level of CYP1B1 protein. A significant inverse association was observed between the expression levels of miR-27b and CYP1B1 protein. Thus, the decreased expression of miR-27b would be one of causes of the high expression of CYP1B1 protein in cancerous tissues. This is the first study to show that miRNAs regulate not only essential genes for physiologic events but also drug-metabolizing enzymes. (Cancer Res 2006; 66(18): 9090-8)

Introduction

MicroRNAs (miRNA) have received attention as a new class of small noncoding RNAs regulating the expression of genes that are involved in various biological processes, such as development, cell proliferation, and apoptosis (1, 2). The number of currently known miRNAs in mammalian has risen dramatically, and their total number in humans has been predicted to be as high as 1,000 (3). Primary miRNA transcripts are cleaved by RNase III Drosha in the cell nucleus into 70-nucleotide to 80-nucleotide precursor miRNA (pre-miRNA) hairpins and transported to the cytoplasm, where pre-miRNAs are processed by RNase III Dicer into 19-nucleotide to 25-nucleotide miRNA duplexes. One strand of duplexes is degraded, and the other strand is used as mature miRNA. Mature miRNAs that are incorporated into the RNA-induced silencing complex recognize the 3′-untranslated region (UTR) of the target mRNA and cause translational repression or mRNA cleavage (4). The functional miRNAs have been predicted to control up to 20% to 30% of the genes within the human genome (5, 6). Recently, several studies have reported that the expression profiles of miRNAs were associated with the development of various types of human tumors. For example, human let-7 miRNA is down-regulated in lung cancers and inhibits the growth of lung cancer cells *in vitro* (7). A recent study indicated that let-7 miRNA controls the post-transcriptional regulation of the RAS oncogene (8). miR-15 and miR-16 were deleted or down-regulated in the majority of B-cell chronic lymphocytic leukemias (9), and the expression levels of miR-143 and miR-145 were decreased in colon cancer tissues as well as in cancer cell lines (10). Some oncogenes have been thought to be the potential target genes of these miRNAs. Thus, the miRNAs may be one of the key regulators of tumorigenesis.

Human cytochrome P450 (CYP) 1B1 is a member of CYP and is mainly expressed in ovary, uterus, and breast (11, 12). CYP1B1 catalyzes the metabolic activation of a variety of procarcinogens and promutagens, including polycyclic aromatic hydrocarbons and aryl amines (12) and metabolism of 17β-estradiol (13–15). Whereas 17β-estradiol contributes to the growth and development of estrogen-dependent cancers, such as breast and endometrial cancers (16), 4-hydroxyestradiol, a catechol metabolite formed by CYP1B1, generates free radicals from reductive-oxidative cycling with the corresponding semiquinone and quinone forms, which cause DNA damage (17, 18). The expression level of CYP1B1 is higher in various types of malignant cancers compared with normal tissues (19). Thus, it is evident that CYP1B1 is associated with cancer. It should be noted that there is no apparent difference in the CYP1B1 mRNA levels between tumor and normal tissues (20, 21). Although there is no direct evidence of lack of association between mRNA and protein of CYP1B1 in panel of human tissues, the phenomena are reminiscent of post-transcriptional regulation. An extremely long 3′-UTR (~3 kb) is peculiar to CYP1B1 mRNA. This background prompted us to investigate whether human CYP1B1 might be post-transcriptionally regulated by miRNA.

Materials and Methods

Chemicals and reagents. The pGL3-promoter vector, phRL-TK plasmid, pTARGET vector, Tfx-20 reagent, and a dual-luciferase reporter assay system were from Promega (Madison, WI). LipofectAMINE and LipofectAMINE 2000 were purchased from Invitrogen (Carlsbad, CA). The *mir*Vana miRNA Probe Construction kit, *mir*Vana miRNA Detection kit, and Pre-miR miRNA Precursors for miR-27b and for negative control were from Ambion (Austin, TX). Antisense 2′-*O*-methyl oligoribonucleotides (AsO) for miR-27b (5′-CAGAACUUAGCCACUGUGAAL, in which L is 3′-aminolinker)

Requests for reprints: Tsuyoshi Yokoi, Drug Metabolism and Toxicology, Division of Pharmaceutical Sciences, Graduate School of Medical Science, Kanazawa University, Kakuma-machi, Kanazawa 920-1192, Japan. Phone: 81-76-234-4407; Fax: 81-76-234-4407; E-mail: tyokoi@kenroku.kanazawa-u.ac.jp.

doi:10.1158/0008-5472.CAN-06-1403

and for negative control (5′-AGACUAGCGGUAUCUUAAACCL) were from Dharmacon (Chicago, IL). All primers and oligonucleotides were commercially synthesized at Hokkaido System Sciences (Sapporo, Japan). Rabbit anti-human CYP1B1 polyclonal antibodies for Western blot analysis and for immunohistochemical analysis were from BD Gentest (Worburn, MA) and Alpha Diagnostic International (San Antonio, TX), respectively. Rabbit anti-human CYP1A1 antibodies and recombinant human CYP1A1 or CYP1B1 expressed in baculovirus-infected insect cells were from BD Gentest. TCDD and G418 were obtained from Cambridge Isotope Laboratories (Cambridge, MA) and Wako Pure Chemicals (Tokyo, Japan), respectively. All other chemicals and solvents were of the highest grade commercially available.

Cells and culture conditions. The human uterine cervix adenocarcinoma cell line HeLa was obtained from Riken Gene Bank (Tsukuba, Japan). The human breast adenocarcinoma cell line MCF-7 and human embryonic kidney cell line HEK293 were obtained from the American Type Culture Collection (Rockville, MD). The human leukemic T-cell line Jurkat was kindly provided by Dr. Yoshinobu Nakanishi (Kanazawa University, Kanazawa, Japan). HeLa cells were cultured in DMEM (Nissui Pharmaceutical, Tokyo, Japan) supplemented with 10% fetal bovine serum (FBS; Invitrogen). MCF-7 cells were cultured in DMEM supplemented with 0.1 mmol/L nonessential amino acid (Invitrogen) and 10% FBS. HEK293 cells were cultured in DMEM supplemented with 4.5 g/L glucose, 10 mmol/L HEPES, and 10% FBS. Jurkat cells were cultured in RPMI 1640 (Nissui Pharmaceutical) supplemented with 10% FBS. These cells were maintained at 37°C under an atmosphere of 5% CO_2-95% air.

RNase protection assay. Total RNA was isolated from the cells using ISOGEN (Nippon Gene, Tokyo, Japan). Antisense RNA probes were synthesized by *mir*Vana miRNA Probe Construction kit. The oligonucleotides used for miR-27b and U6 small nuclear RNA (snRNA) were 5′-TTCACAGTGGCTAAGTTCTGCCTGTCTC-3′ and 5′-AGAAGATTAGCATGGCCCCTGCGCAAGGCCTGTCTC-3′, respectively. RNase protection assays were done using a *mir*Vana miRNA Detection kit according to the manufacturer's protocol. The antisense RNA probes labeled with [α-^{32}P]UTP using T7 RNA polymerase were hybridized to total RNA (3 μg) at 42°C for 10 hours and then digested by RNase A/T1. The protected miRNAs were separated by electrophoresis through 15% polyacrylamide/1× Tris-borate EDTA (TBE)/8 mol/L urea gels with 1× TBE as the running buffer, and then the miRNAs were detected and quantified with a Fuji Bio-Imaging Analyzer BAS 1000 (Fuji Film, Tokyo, Japan).

Real-time reverse transcription-PCR. The cDNAs were synthesized from total RNAs using ReverTra Ace (Toyobo, Osaka, Japan) according to the manufacturer's protocol. The forward and reverse primers for human precursor miR-27b (pre-miR-27b) were 5′-ACCTCTCTAACAAGGTGCAGAGCTT-3′ and 5′-ACCTTCTCTTCAGGTGCAGAACTTAG-3′, respectively. The forward and reverse primers for human U6 snRNA were 5′-CGCTTCGGCAGCACATATACTAA-3′ and 5′-TATGGAACGCTTCACGAATTTGC-3′, respectively. The PCR analyses for human pre-miR-27b were done as follows: after an initial denaturation at 95°C for 30 seconds, the amplification was done by denaturation at 95°C for 10 seconds, annealing and extension at 68°C for 20 seconds for 45 cycles. The PCR condition for human U6 snRNA was done as follows: after an initial denaturation at 95°C for 30 seconds, the amplification was done by denaturation at 94°C for 10 seconds, annealing and extension at 62°C for 20 seconds for 45 cycles. PCR was done using the Smart Cycler (Cepheid, Sunnyvale, CA) with Smart Cycler software (version 1.2b).

Construction of reporter plasmids. To construct luciferase reporter plasmids, various target fragments were inserted at the *Xba*I site, downstream of the luciferase gene in the pGL3-promoter vector. The sequence from +4,358 to +4,381 in the human *CYP1B1* gene (5′-CAGAACTTAGCCTTTACCTGTGAA-3′) was termed miR-27b recognition element (MRE27b). The fragment containing three copies of the MRE27b, 5′-CTAGATTCATGTCC-*CAGAACTTAGCCTTTACCTGTGAA*GTGTTCATGTCC*CAGAACTTAGCCTTTACCTGTGAA*GTGTTCATGTCC*CAGAACTTAGCCTTTACCTGTGAA*GTG-3′ (MRE27b is italicized), was cloned into the pGL3-promoter vector, resulting in single and double insertions. These plasmids were termed pGL3/1B1MREx3 and pGL3/1B1MREx6, respectively. A fragment containing the perfect matching sequence with the mature miR-27b, 5′-CTAGA*CAGAACTTAGCCACTGTGAA*T-3′ (the matching sequence of miR-27b is italicized), was cloned into the pGL3-promoter vector (pGL3/miR-27b). The region 1 (+4,311 to +4,439) containing the MRE27b and the region 2 (+3,899 to +4,019) in the human *CYP1B1* gene (Fig. 1*A*) were amplified by PCR using the following primers adapted to the *Xba*I site: 5′-TTTTCTAGATGTCTCAGGTTTGTTTT-3′ and 5′-GAATCTAGAATGCAACTATTTGATCT-3′ for region 1 and 5′-GCTCTAGATGCCTCATTATGTCAACCA-3′ and 5′-GCTCTAGACCTTACCTTTCTTCCATATAAA-3′ for region 2. The pGL3-promoter plasmids containing regions 1 and 2 were termed pGL3/1B1UTR1 and pGL3/1B1UTR2 plasmids, respectively. The complementary sequence of region 1 was also cloned into the pGL3-promoter plasmid (pGL3/1B1UTR1rev). The nucleotide sequences of the constructed plasmids were confirmed by DNA sequencing analyses.

Luciferase assay. For luciferase assays, various luciferase reporter plasmids (pGL3) were transiently transfected with phRL-TK plasmid into MCF-7 and Jurkat cells. Briefly, the day before transfection, the cells were seeded into 24-well plates, and 24 hours later, 380 ng of pGL3 plasmid and 20 ng of phRL-TK plasmid were transfected using Tfx-20 reagent for MCF-7 cells or LipofectAMINE 2000 for Jurkat cells. In some cases, various doses of the precursors for miR-27b or control or the AsOs for miR-27b or control were cotransfected with reporter plasmids. After incubation for 48 hours,

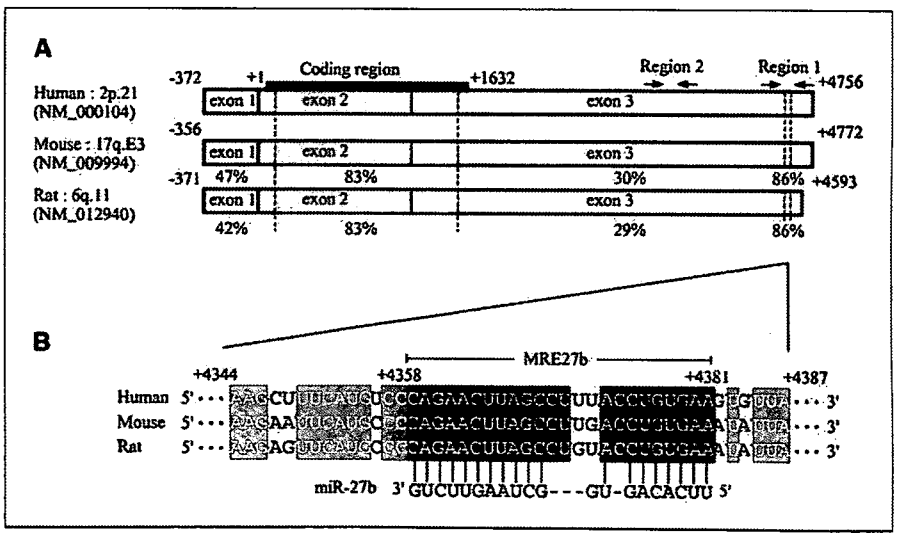

Figure 1. Homology between CYP1B1 mRNAs and the predicted target sequence of miR-27b. *A*, CYP1B1 mRNA in human, mouse, and rat. *Parentheses*, accession numbers. CYP1B1 mRNAs are 5.0 to 5.2 kb in length and consist of three exons. The numbering refers to the ATG in translation starting with A as 1, and the coding region of human CYP1B1 is up to +1,632. *Gray*, highly conserved regions. Homology to each region of human CYP1B1 mRNA. *Arrows*, location and direction of PCR primers for amplification of regions 1 (+4,311 to +4,439) and 2 (+3,899 to +4,019). *B*, sequence of MRE27b is located on +4,358 to +4,381 in the 3′-UTR of human CYP1B1 mRNA. *Gray boxes*, conserved nucleotides; *black boxes*, MRE27b.

the cells were resuspended in passive lysis buffer and then the luciferase activity was measured with a luminometer (Wallac, Turku, Finland) using the dual-luciferase reporter assay system.

Stable expression of recombinant human CYP1B1 in HEK293 cells. A fragment containing the full-length coding region and 3′-UTR of human *CYP1B1* cDNA (from −21 to +4,756) was amplified by PCR using the primers of 5′-GAAACCGCACCTCCCCG-3′ and 5′-AAAGTATATTAAA-CAAAGTTTC-3′. It was subcloned into the pTARGET vector. The nucleotide sequences of the plasmid (pTARGET/CYP1B1) were confirmed by DNA sequencing analyses. HEK293 cells were seeded into six-well plates, and 2 μg of pTARGET/CYP1B1 plasmid were transfected using LipofectAMINE according to the manufacturer's protocols. When the cells reached 60% confluence, they were diluted from 1:10 to 1:200 and subjected to 400 μg/mL G418. The medium was renewed every week, and colonies of stably transfected cells (HEK293/1B1 cells) were isolated and expanded.

Electroporation of AsO and precursor for miR-27b. MCF-7 and HEK293/1B1 cells were washed twice with PBS and resuspended in HEPES-buffered saline [10 mmol/L HEPES (pH 7.3), 140 mmol/L NaCl] with 6 mmol/L glucose at 6×10^5 and 1×10^6 cells per pulse, respectively. A 250-μL aliquot of cells was added to a 0.4-cm gap electroporation cuvette (Bio-Rad, Hercules, CA) with 75, 125, 750, or 1,125 pmol of AsOs or 50, 100, 200, or 400 pmol of precursor and then incubated at 4°C for 10 minutes. The cells were then electroporated using a Gene Pulser II (Bio-Rad) at 220 V and 950 μF for MCF-7 cells and at 245 V and 950 μF for HEK293/1B1 cells and grown in the medium for 24 to 96 hours. After the incubation, the protein level and enzymatic activity of CYP1B1 were determined as described below.

SDS-PAGE and Western blot analyses. To prepare microsomes, MCF-7 cells seeded into 10-cm dishes were harvested and homogenized with homogenization buffer [0.1 mol/L Tris-HCl, 0.1 mol/L KCl, 1 mmol/L EDTA (pH 7.4)] and centrifuged at 19,000 × *g*, 4°C for 20 minutes. The supernatant was centrifuged at 105,000 × *g* for 1 hour at 4°C, and the precipitate was resuspended in TGE buffer [10 mmol/L Tris-HCl, 20% glycerol, 1 mmol/L EDTA (pH 7.4)]. To prepare the whole-cell lysate, HEK293/1B1 cells seeded into 10-cm dishes were harvested and homogenized with lysis solution [8 mol/L urea, 4% CHAPS, 2% Pharmalyte (pH 3-10)] containing protease inhibitors (1 mmol/L DTT, 0.5 mmol/L amidinophenyl methanesulfonyl fluoride hydrochloride, 2 μg/mL aprotinin, 2 μg/mL pepstatin, 2 μg/mL leupeptin). After centrifuging at 12,000 × *g* for 1 hour at 4°C, the supernatant was collected. The microsomal protein (30 μg) or whole-cell lysate (10 μg) was separated by 7.5% SDS-PAGE. The gel was transferred onto nitrocellulose membrane and probed with rabbit anti-human CYP1B1 or rabbit anti-human CYP1A1 antibodies. Biotinylated anti-rabbit IgG and Vectastain avidin-biotin complex method (ABC) kit (Vector Laboratories, Burlingame, CA) were used for diaminobenzidine staining.

Enzymatic activity. The enzymatic activity of CYP1B1 was determined using a P450-Glo Assay kit (Promega). After the electroporation, the cells seeded into 24-well plates were treated with 10 nmol/L TCDD for the last 24 hours, and then the medium was replaced with medium containing 20 μmol/L Luciferin 6′ chloroethyl ether. After incubation for 8 hours at 37°C under an atmosphere of 5% CO_2-95% air, 100 μL of the medium were added to 100 μL of Luciferin Detection Reagent. After incubation for 20 minutes at room temperature, the luminescence was measured with a luminometer. The protein concentrations of the cells were determined using Bradford protein assay reagent (Bio-Rad) with γ-globulin as the standard. The enzymatic activity was normalized with the protein content.

Human breast cancerous and adjacent noncancerous tissues. Breast cancerous and adjacent noncancerous tissues were obtained as surgical samples from 24 Japanese patients with primary breast carcinoma. The patients (ages 41-77 years) were nonsmokers and had not undergone chemotherapy. By standard histopathologic criteria, 21 patients were diagnosed as invasive ductal carcinoma and 3 patients as invasive lobular carcinoma. The histologic grade was determined by standard criteria (22) as grade 1 (n = 1), grades 1 to 2 (n = 13), grade 2 (n = 9), and grades 2 to 3 (n = 1). The samples were obtained immediately after resection, divided into breast cancerous and adjacent noncancerous tissues, and immediately frozen with liquid nitrogen. The samples were stored at −80°C until use. The expression levels of miR-27b in human breast cancerous and adjacent noncancerous tissues were determined by RNase protection assay and real-time reverse transcription-PCR (RT-PCR) as described above. This study was approved by the Ethics Committee of Kanazawa University. Written informed consent was obtained from all subjects before their participation in this study.

Immunohistochemistry. Immunohistochemical analyses of CYP1B1 were done using formalin-fixed, paraffin-embedded specimens of breast cancerous tissues from 24 patients. The sections were soaked in Antigen Retrieval Citra Solution (BioGenex, San Ramon, CA) at room temperature for 10 minutes and then incubated with anti-human CYP1B1 antibodies at 4°C for 16 hours. About the antibodies, no significant cross-reactivity to either human CYP1A1 or CYP1A2 protein has been reported (23). Staining was done using a Vectastain ABC kit. The extent of immunostaining was evaluated by the intensity of staining (score, 1-3), the localization in cytoplasm (score, 1-3), and area of staining (score, 1-4). Based on the combined scores, the samples were divided into three groups as weak (score, 3-5), moderate (score, 6-7), and strong (score, 8-10) staining of CYP1B1 protein. Three independent pathologists judged the results.

Statistical analyses. Data are expressed as mean ± SD of triplicate determinations. Statistical significance was determined by ANOVA and Dunnett multiple comparisons test. Comparison of two groups was made with an unpaired, two-tailed Student's t test. Correlations between the results obtained by RNase protection assay and real-time RT-PCR were determined by Pearson's product-moment method. The statistical significance of differences between the expression level of miR-27b in breast cancerous tissues and adjacent noncancerous tissues was determined by paired, two-tailed Student's t test. The relationships between the immunostained CYP1B1 level and miR-27b level in human breast cancerous tissues were investigated by ANOVA and Tukey method test. A $P < 0.05$ was considered statistically significant.

Results

A miR-27b complementary sequence on the 3′-UTR of human CYP1B1 mRNA. In the human CYP1B1 mRNA (5.2 kb), the 3′-UTR is extremely long (~3 kb; Fig. 1*A*). When the sequences of the CYP1B1 mRNA were compared between human, mouse, and rat, the homology of the coding region was extremely high (>80%). In addition, high homology was found in the 3′-UTR near the polyadenylation site of 44 nucleotides in length (from +4,344 to +4,387). A near-perfect matching sequence with miR-27b was identified (from +4,358 to +4,381) using the miRNA registry release 7.1 (Fig. 1*B*; ref. 24).[3] This region was termed the miR-27b recognition element (MRE27b). We investigated whether miR-27b might be involved in the regulation of human CYP1B1 expression through the MRE27b.

Expression levels of miR-27b in human cancer cell lines. A RNase protection assay was done to determine the expression level of mature miR-27b in various human cancer cell lines (Fig. 2*A*). The mature miR-27b was detected in HeLa and MCF-7 cells but not in Jurkat and HEK293 cells. The expression level of pre-miR-27b was determined by real-time RT-PCR (Fig. 2*B*). Consistently, HeLa and MCF-7 cells showed significantly high expression of pre-miR-27b compared with Jurkat and HEK293 cells.

Luciferase assays in MCF-7 or Jurkat cells. Luciferase assays were done using various reporter constructs in MCF-7 and Jurkat cells (Fig. 2*C*). In miR-27b-positive MCF-7 cells, the reporter activity of the pGL3/miR-27b plasmid was significantly lower than that of the pGL3-promoter plasmid. The reporter activities of the pGL3/1B1MREx3 and pGL3/1B1MREx6 plasmids containing multiple

[3] http://www.sanger.ac.uk/Software/Rfam/mirna/.

copies of MRE27b were also significantly lower than that of pGL3-promoter plasmid. In addition, the pGL3/1B1UTR1 plasmid showed significantly lower reporter activity but the pGL3/1B1UTR1rev and pGL3/1B1UTR2 plasmids did not. In contrast, only the reporter activity of the pGL3/1B1MREx6 plasmid was decreased in miR-27b-negative Jurkat cells. These results suggest that the 3′-UTR of human CYP1B1 represses the activity in association with the expression of miR-27b.

Effects of overexpression or inhibition of miR-27b on luciferase activity. To investigate whether miR-27b might control the luciferase activity, the precursor for miR-27b was exogenously expressed in Jurkat cells (Fig. 2*D* and *E*). The overexpression of miR-27b significantly decreased the luciferase activities of the pGL3/miR-27b (17% of control), pGL3/1B1MREx3 (34% of control), pGL3/1B1MREx6 (26% of control), and pGL3/1B1UTR1 (62% of control) plasmids (Fig. 2*D*). As shown in Fig. 2*E*, the precursor for

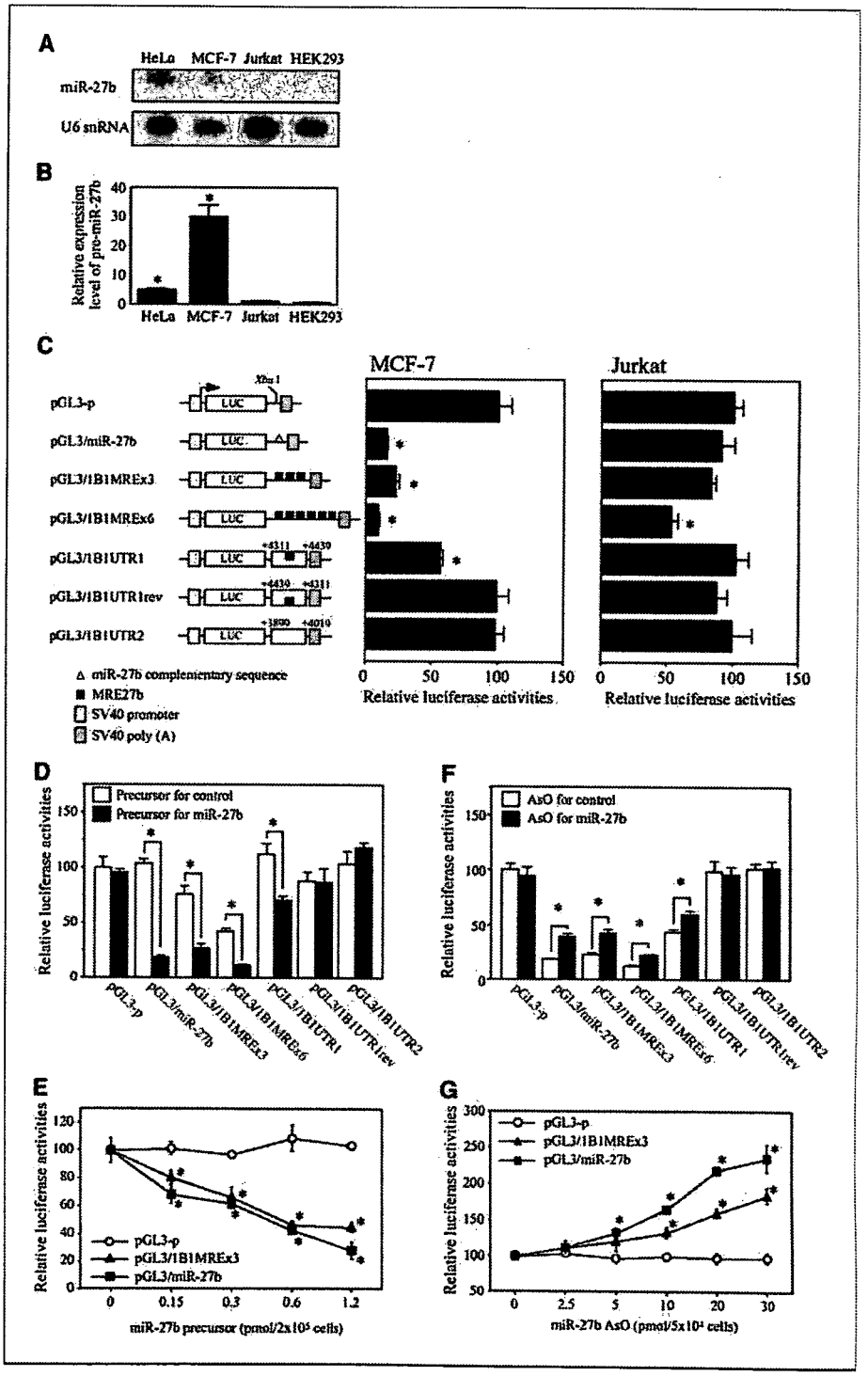

Figure 2. Expression level of miR-27b in various human cancer cell lines and luciferase assays with reporter constructs containing MRE27b in human CYP1B1 in MCF-7 and Jurkat cells. *A*, expression levels of mature miR-27b in HeLa, MCF-7, Jurkat, and HEK293 cells were determined by RNase protection assay. U6 snRNA was used as a loading control. *B*, expression of pre-miR-27b in cells was determined by real-time RT-PCR. Values are the pre-miR-27b level normalized with the U6 snRNA level relative to that in Jurkat cells. *Columns*, mean of three independent experiments; *bars*, SD. *, $P < 0.01$, compared with Jurkat cells. *C*, a series of reporter constructs containing the 3′-UTR of the human *CYP1B1* gene was transiently transfected into MCF-7 or Jurkat cells. Relative luciferase activities were normalized with the *Renilla* luciferase activities. Values are expressed as percentages of the relative luciferase activity of pGL3-promoter plasmid. *Columns*, mean of three independent experiments; *bars*, SD. *, $P < 0.01$, compared with pGL3-promoter. *D*, a series of reporter constructs containing the 3′-UTR of the human *CYP1B1* gene was transiently transfected into Jurkat cells with 1.2 pmol/2 × 10^5 cells of the precursors for miR-27b or control. *E*, various concentrations of the precursors for miR-27b were transiently transfected into Jurkat cells with luciferase reporter plasmids. *F*, a series of reporter constructs containing the 3′-UTR of the *CYP1B1* gene was transiently transfected into MCF-7 cells with 30 pmol/5 × 10^4 cells of the AsO for miR-27b or control. *G*, various concentration of the AsO for miR-27b were transiently transfected into MCF-7 cells with luciferase reporter plasmids. Relative luciferase activity was normalized to the *Renilla* luciferase activity. *Points*, mean of three independent experiments; *bars*, SD. *, $P < 0.01$, compared with the precursor for control or the AsO for control (*D* and *F*). *, $P < 0.01$, compared with pGL3-promoter without precursor or AsO (*E* and *G*).

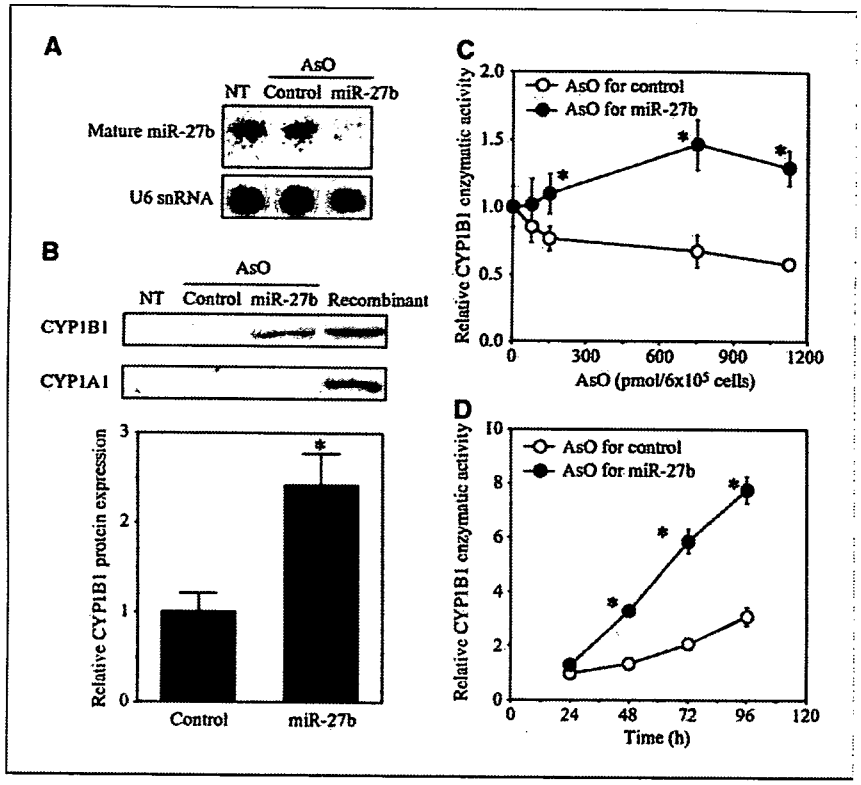

Figure 3. Effects of AsO for miR-27b on the protein level and enzymatic activity of endogenous CYP1B1 in MCF-7 cells. *A* and *B*, AsOs for miR-27b or control (750 pmol/6 × 10^5 cells) were electroporated into MCF-7 cells. After 72 hours, the cells were harvested and total RNA and microsomes were isolated. *A*, expression levels of mature miR-27b and U6 snRNA were determined by RNase protection assays. *B*, expression levels of CYP1B1 and CYP1A1 protein were determined by Western blot analyses. The recombinant human CYP1B1 protein (50 fmol) and CYP1A1 protein (50 fmol) were used as controls. *Columns*, mean of three independent experiments; *bars*, SD. *, $P < 0.01$, compared with the AsO for control. *C*, various concentrations of the AsOs for miR-27b or control were electroporated into MCF-7. After 72 hours, the CYP1B1 enzymatic activities were determined by P450-Glo assay. Values are expressed relative to the activity without AsO. *Points*, mean of three independent experiments; *bars*, SD. *, $P < 0.01$, compared with the AsO for control. *D*, after the electroporation with 750 pmol/6 × 10^5 cells of the AsOs for miR-27b or control, the MCF-7 cells were incubated for 24 to 96 hours and then the enzymatic activities were measured. Values are expressed relative to the activity with AsO for 24 hours. *Points*, mean of three independent experiments; *bars*, SD. *, $P < 0.01$, compared with the AsO for control.

miR-27b decreased the luciferase activities of pGL3/miR-27b and pGL3/1B1MREx3 plasmids in a concentration-dependent manner.

To investigate the effect of inhibition of endogenous miR-27b on the luciferase activity, AsO for miR-27b was transfected in MCF-7 cells (Fig. 2*F* and *G*). The transiently transfected AsO for miR-27b significantly increased the luciferase activities of the pGL3/miR-27b (2.1-fold of control), pGL3/1B1MREx3 (1.8-fold of control), pGL3/1B1MREx6 (1.8-fold of control), and pGL3/1B1UTR1 plasmids (1.4-fold of control; Fig. 2*F*). As shown in Fig. 2*G*, the AsO for miR-27b increased the luciferase activities of pGL3/miR-27b and pGL3/1B1MREx3 plasmids in a concentration-dependent manner. These results suggest that miR-27b recognized the MRE27b on the human CYP1B1 mRNA and regulated the expression post-transcriptionally.

Effects of inhibition of miR-27b on protein level and enzymatic activity of endogenous CYP1B1 in MCF-7 cells. We investigated the effects of the inhibition of miR-27b on the protein level and enzymatic activity of endogenous CYP1B1. A RNase protection assay revealed that the endogenous miR-27b level was greatly decreased by the transfection of the AsO for miR-27b in MCF-7 cells (Fig. 3*A*). As shown in Fig. 3*B*, the CYP1B1 protein level was significantly increased by the transfection of the AsO for miR-27b. That there was no change of the CYP1A1 protein level indicated that the effects of the AsO for miR-27b were specific for CYP1B1 protein. The effects of the AsO for miR-27b on the enzymatic activity of CYP1B1 were examined by a P450-Glo assay. The enzymatic activity of CYP1B1 was increased by the electroporation of the AsO for miR-27b in MCF-7 cells in concentration- and time-dependent manners (Fig. 3*C* and *D*).

Effects of overexpression of miR-27b on protein level and enzymatic activity of exogenous CYP1B1 in HEK293 cells. HEK293/1B1 cells were used to investigate the effects of overexpression of miR-27b on the protein level and enzymatic activity of CYP1B1. A RNase protection assay revealed that the miR-27b level was greatly increased by the transfection of the precursor for miR-27b in HEK293/1B1 cells (Fig. 4*A*). As shown in Fig. 4*B*, the CYP1B1 protein level was significantly decreased by the transfection of the precursor for miR-27b. P450-Glo assays showed that the enzymatic activity of CYP1B1 was decreased by the electroporation of the precursor for miR-27b in HEK293/1B1 cells in a concentration-dependent manner (Fig. 4*C*). These results suggest that miR-27b regulates the protein level and enzymatic activity of CYP1B1.

CYP1B1 protein level in human breast cancer. To investigate whether miR-27b affects the CYP1B1 expression *in vivo*, the expression levels of CYP1B1 protein in breast cancerous tissues from 24 patients were determined by immunohistochemistry (Fig. 5). All of breast cancers showed positive immunoreactivity for CYP1B1, and in each case, CYP1B1 was specifically localized to cancer cells. In most samples, the CYP1B1 protein was localized in the cytoplasm, but in some samples, the nuclei were also stained. The extent of staining varied among samples (Fig. 5*A* to *C*). According to the scoring, samples from 6, 11, and 7 patients were categorized to groups I (weak staining), II (moderate staining), and III (strong staining), respectively. No staining was observed in normal rabbit IgG (Fig. 5*D*).

Inverse association between expression level of miR-27b and CYP1B1 protein in human breast cancer. RNase protection assays require abundant RNA compared with real-time RT-PCR. Because the RNA quantities obtained from human samples were limited, we investigated whether the pre-miR-27b level determined by real-time RT-PCR can substitute for the mature miR-27b levels determined by RNase protection assay. Breast cancerous and adjacent noncancerous tissues from 11 patients were used for RNase protection assay and real-time RT-PCR analysis. Figure 6*A*

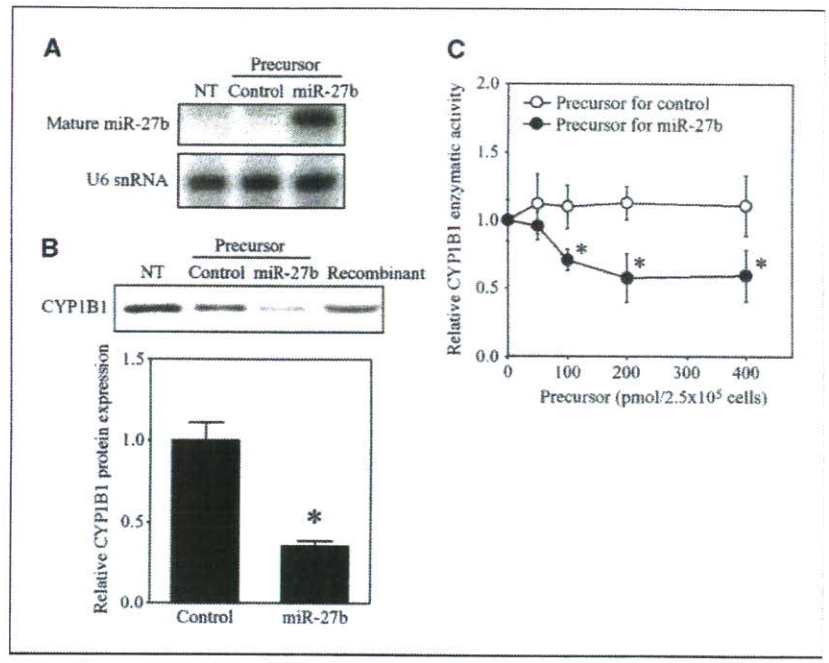

Figure 4. Effects of precursor for miR-27b on protein level and enzymatic activity of exogenous CYP1B1 in HEK293/1B1 cells. *A* and *B*, precursors for miR-27b or control (200 pmol/2.5 × 10^5 cells) were electroporated into HEK293/1B1 cells. After 48 hours, the cells were harvested and total RNA and whole-cell lysate were isolated. *A*, expression levels of mature miR-27b and U6 snRNA were determined by RNase protection assays. *B*, expression levels of CYP1B1 protein was determined by Western blot analysis. Recombinant human CYP1B1 protein (500 fmol) was used as a control. *Columns*, mean of three independent experiments; *bars*, SD. *, $P < 0.001$, compared with the precursor for control. *C*, various concentrations of the precursors for miR-27b or control were electroporated into HEK293/1B1 cells. After 48 hours, the CYP1B1 enzymatic activities were determined by P450-Glo assay. Values are expressed relative to the activity without precursor. *Points*, mean of three independent experiments; *bars*, SD. *, $P < 0.05$, compared with the precursor for control.

shows a typical autoradiogram of the mature miR-27b levels in four patients. In three of four patients, the mature miR-27b levels in the cancer tissues were lower than those in noncancerous tissues. A significant correlation ($r = 0.700$; $P < 0.0005$) was observed between the mature miR-27b levels and pre-miR-27b levels (Fig. 6*B*). In addition, a significant correlation ($r = 0.720$; $P < 0.0005$) was observed between the U6 snRNA levels determined by the RNase protection assay and those determined by real-time RT-PCR. Accordingly, we evaluated the miR-27b level normalized with U6 snRNA in breast cancerous and adjacent noncancerous tissues from 24 patients by real-time RT-PCR. Consequently, it was clearly shown that the expression level of pre-miR-27b in cancerous tissues (0.48-4.55, 1.52 ± 0.99) was significantly ($P < 0.0005$) lower than that in noncancerous tissues (1.28-5.71, 2.66 ± 1.06; Fig. 6*C*).

We investigated the relationship between the miR-27b level and CYP1B1 protein level in human breast cancers (Fig. 6*D*). The expression levels of pre-miR-27b in each group were as follows: group I (2.49 ± 1.25), group II (1.43 ± 0.72), and group III

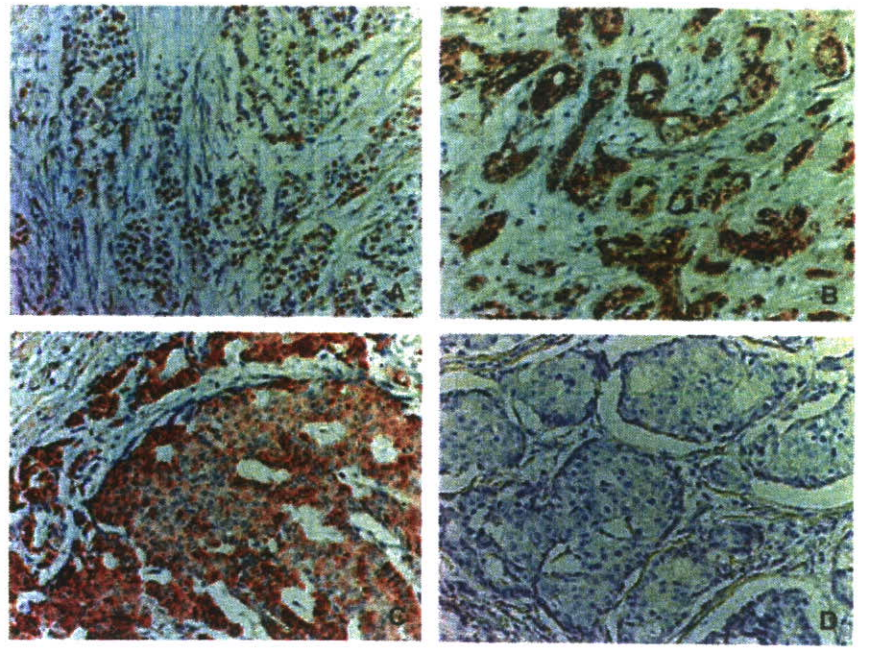

Figure 5. Immunohistochemical staining of CYP1B1 protein in breast cancerous tissues. Immunohistochemical analyses were done in human breast cancerous tissues using anti-human CYP1B1 antibodies. *A*, grades 1 to 2 invasive ductal carcinoma. CYP1B1 immunostaining is weakly detected in the nucleus (score 3). *B*, grades 1 to 2 invasive ductal carcinoma. CYP1B1 immunostaining is moderately observed in the cytoplasm and nucleus (score 6). *C*, grade 2 invasive ductal carcinoma. Strong immunostaining of CYP1B1 in the cytoplasm was observed (score 8). *D*, there was no staining with normal rabbit IgG. Original magnification, ×200.

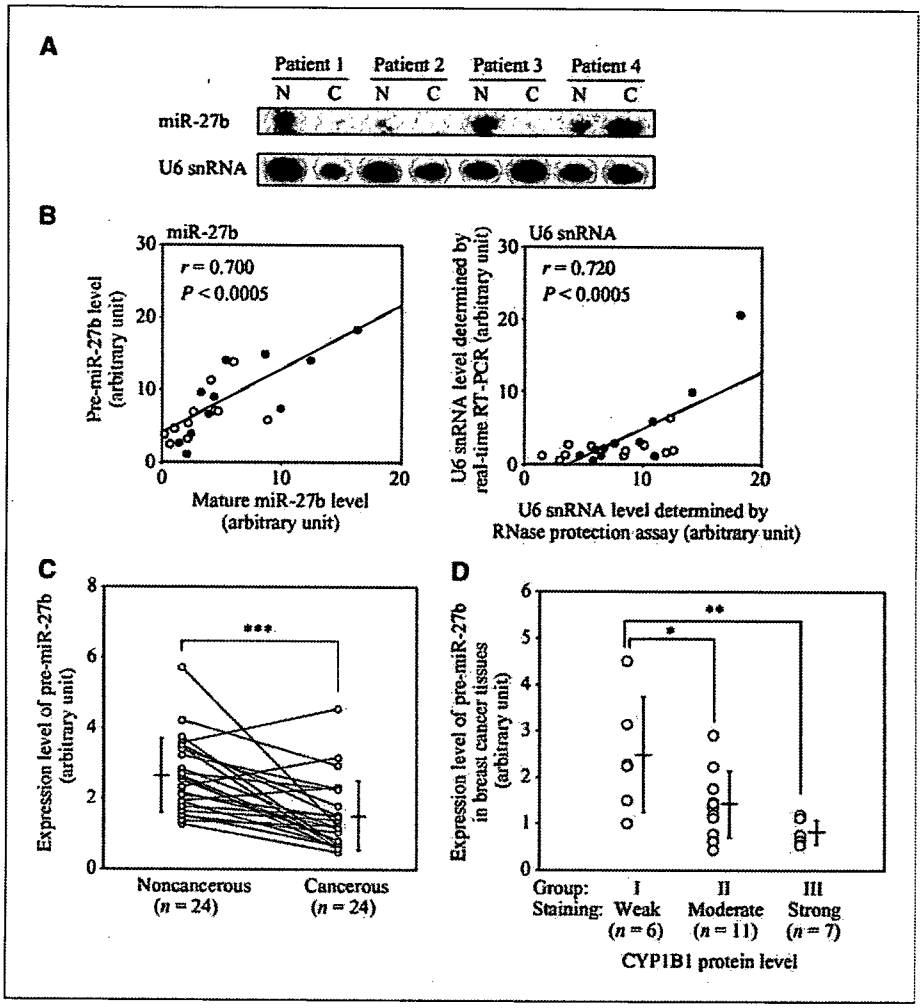

Figure 6. Expression of miR-27b in human breast cancerous tissues and relationship with CYP1B1 protein level. *A*, expression levels of mature miR-27b in breast cancerous (*C*) and adjacent noncancerous (*N*) tissues from four patients were determined by RNase protection assay. U6 snRNA was used as a loading control. *B, left,* correlation was observed between the mature miR-27b levels and pre-miR-27b; *right,* correlation was observed between the expression levels of U6 snRNA determined by RNase protection assay and real-time RT-PCR. Breast cancerous (●) and noncancerous tissues (○) from 11 patients were analyzed. *C,* comparison between the expression levels of pre-miR-27b in breast cancerous and adjacent noncancerous tissues obtained from 24 patients. Expression level of pre-miR-27b was determined by real-time RT-PCR and normalized with U6 snRNA level. *Horizontal bars,* mean; *bars,* SD. ***, $P < 0.0005$, paired Student's *t* test. *D,* inverse association between the expression levels of miR-27b and CYP1B1 protein in human breast cancer. According to the scoring of CYP1B1 immunohistochemistry, 24 samples were divided to three groups: group I (weak staining, 6 samples), group II (moderate staining, 11 samples), and group III (strong staining, 7 samples). *Y axis,* expression level of pre-miR-27b normalized with U6 snRNA in breast cancerous tissues. *Horizontal bars,* mean; *bars,* SD, *, $P < 0.05$; **, $P < 0.01$.

(0.82 ± 0.27). Significant differences were observed between groups I and II ($P < 0.05$) or III ($P < 0.01$). Thus, an inverse association was observed between the expression level of miR-27b and the CYP1B1 protein level in human breast cancer. In contrast to the CYP1B1 protein level, no relationship was observed between the CYP1B1 mRNA level and the miR-27b level in human breast tissues (data not shown). These results suggested that CYP1B1 is post-transcriptionally regulated by miR-27b. The decreased expression of miR-27b would be one of the causes of the high expression of CYP1B1 protein in cancerous tissues.

Discussion

miRNAs are a recently discovered family of short noncoding RNA whose final product is a ~22-nucleotide functional RNA molecule. They play important roles in the regulation of target genes by binding to complementary regions of transcripts to repress their translation or regulate degradation. As many as 1,000 miRNA genes are thought to exist in the human genome (3). Some miRNAs are reported to be associated with physiologic functions, such as differentiation, development, and disease. Because miRNAs have only very recently received attention, the target genes of miRNAs are not completely understood yet. In the present study, we examined whether human CYP1B1, which is a member of CYP and catalyzes the metabolism of procarcinogens and estradiol, might be a target of miRNA.

We identified MRE27b in the 3′-UTR in CYP1B1 mRNA. Luciferase assays showed that the endogenous and exogenous miR-27b negatively regulated the activity through MRE27b. The AsO for miR-27b could restore the protein level and enzymatic activity of endogenous CYP1B1, whereas the precursor for miR-27b decreased the protein expression and enzymatic activity of exogenous CYP1B1. These results clearly indicated that the expression of human CYP1B1 is post-transcriptionally regulated by miR-27b. It is well known that CYP1B1 is transcriptionally regulated, as we (25–27) and others (28–30) previously reported the involvement of aryl hydrocarbon receptor, Sp1, estrogen receptor, and steroidogenic factor-1. Thus, in addition to the transcriptional regulation, we found that the post-transcriptional regulation is also responsible for the CYP1B1 expression. The sequences of mRNA around MRE27b are highly conserved among species (Fig. 1). Therefore, the regulation by miR-27b may occur in other species.

miR-27b is highly expressed in human normal breast (31). Recent studies have reported that the miRNA expression levels are changed with the development of tumors, such as those of lung cancer (7), chronic lymphocytic leukemias (9), colorectal neoplasia (10), large cell lymphoma (32), and glioblastoma (33). Thus, many miRNAs are differentially expressed in different cancers. The